Large-scale shell-model studies for exotic nuclei: probing shell evolution

Yutaka Utsuno

Advanced Science Research Center, Japan Atomic Energy Agency

Center for Nuclear Study, University of Tokyo

In collaboration with

T. Otsuka (Tokyo), N. Shimizu (CNS), Y. Tsunoda (Tokyo),

T. Abe (Tokyo), M. Honma (Aizu), T. Mizusaki (Senshu), T. Togashi (CNS), B. A. Brown (MSU)

Shell evolution: a key property of exotic nuclei

- Shell structure
  - Important not only in single-particle energy levels but also in collectivity
  - Sharp change in exotic nuclei, called shell evolution, is suggested.
- How to deduce the shell evolution?
  - Follow the change of "single-particle energies" along a long isotope chain.
- Purity of single-particle (SP) states
  - Controversial levels in Sb (Z=51) isotopes
    - SP (Schiffer et al., 2004) or coupling to collective (Sorlin and Porquet, 2008)

Many-body calculations with a suitable shell-evolution mechanism are needed.

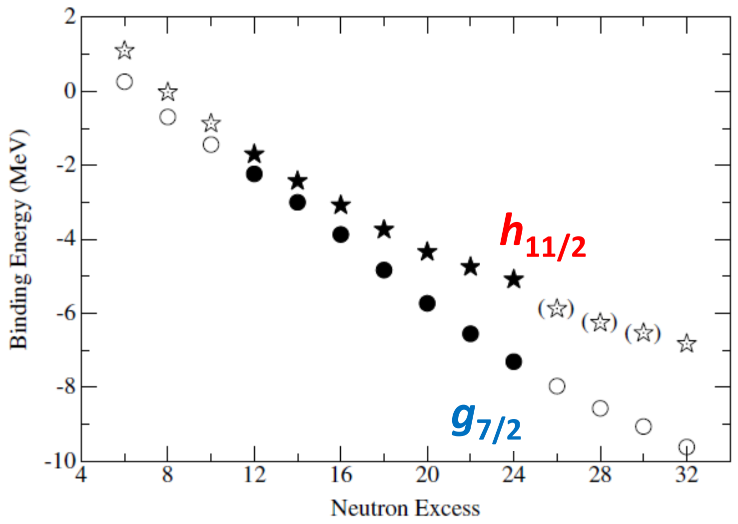

J. P. Schiffer et al., Phys. Rev. Lett. 92, 162501 (2004).

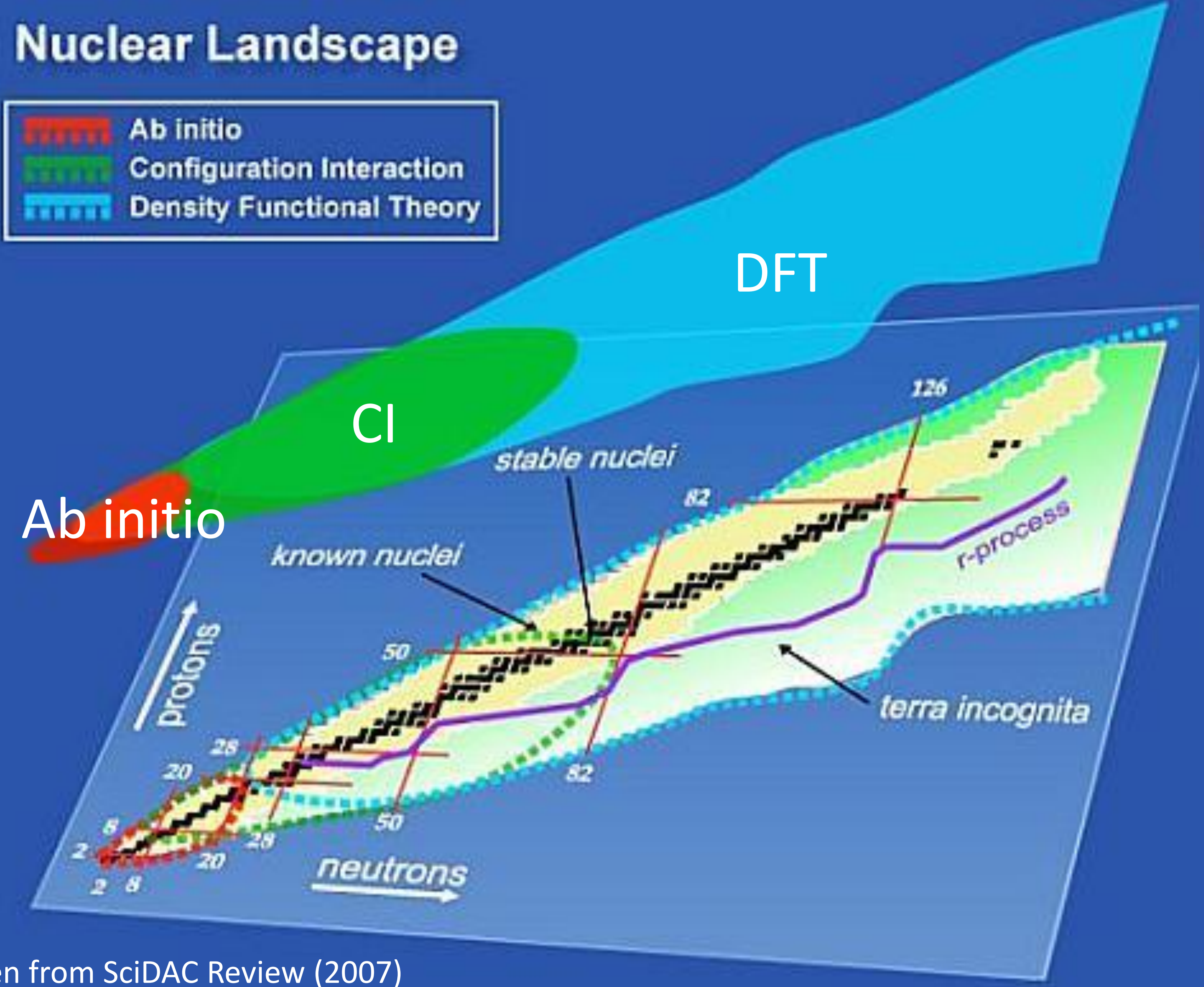

Taken from SciDAC Review (2007)

Computational strategy

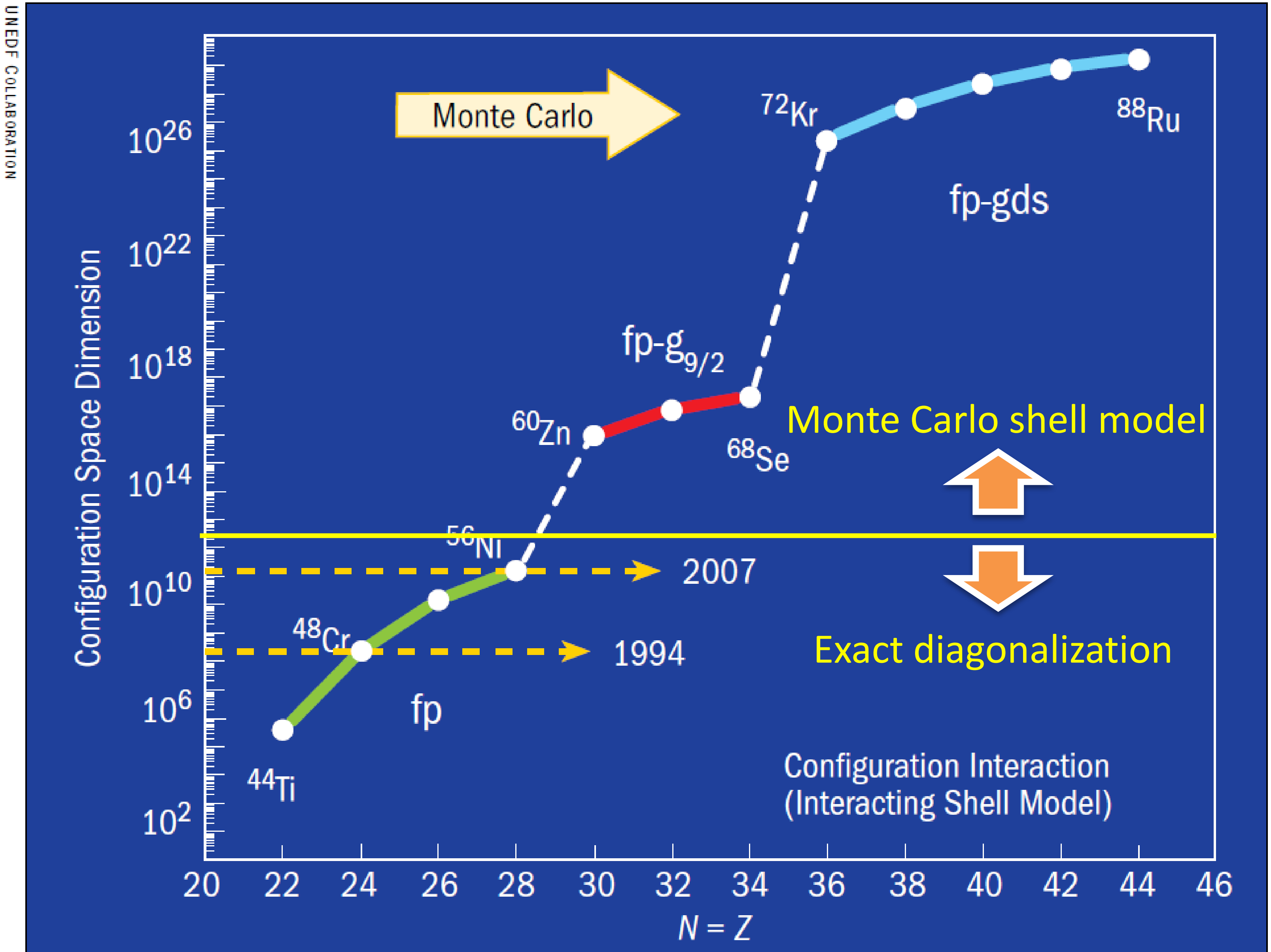

Two major sources of evolution in *p*-*n* channel

- Central and tensor effective forces

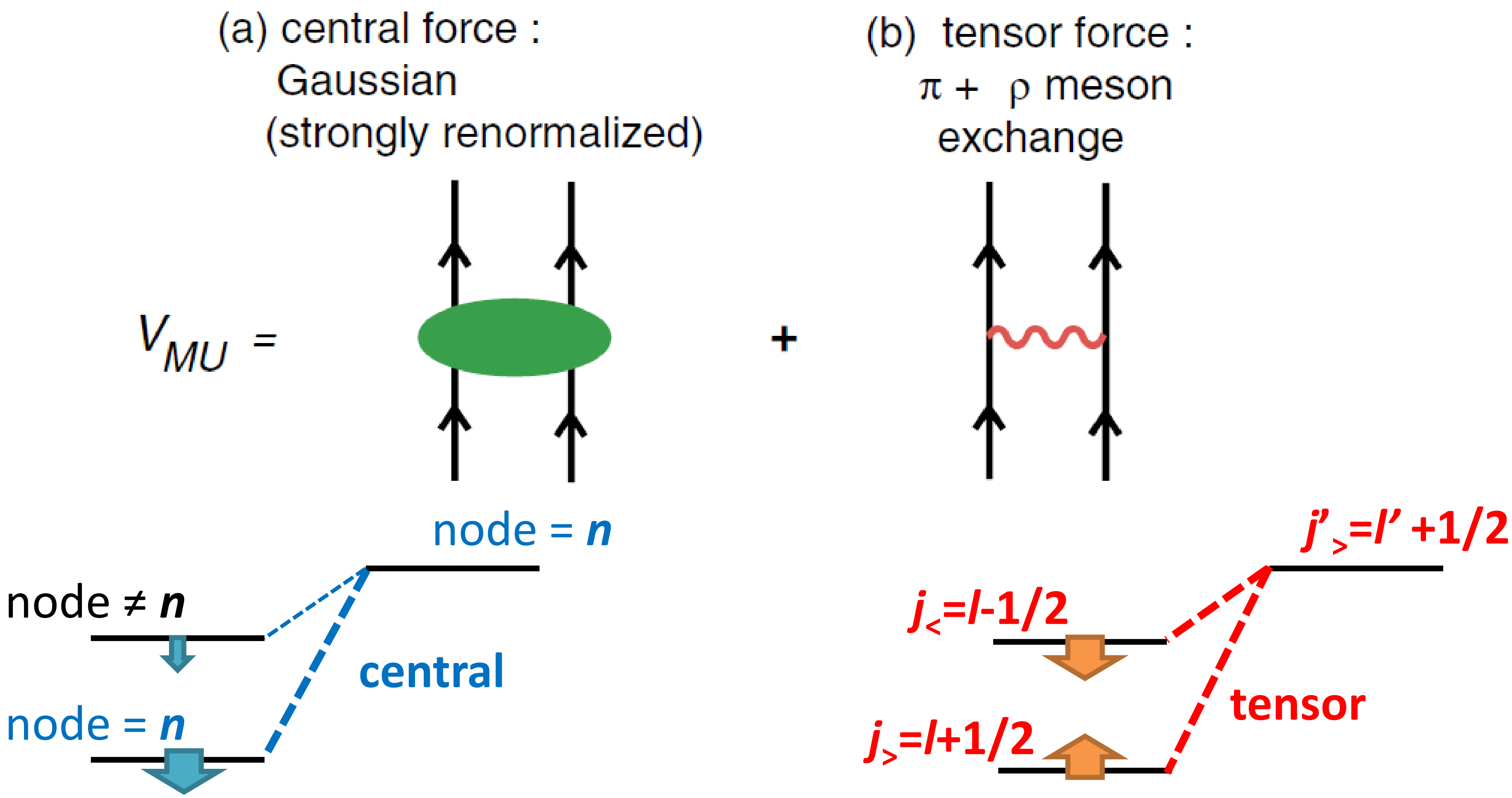

$$(2j_> + 1)V^T_{j_>,j'} + (2j_< + 1)V^T_{j_<,j'} = 0,$$

known for several decades

known for a decade (Otsuka et al., 2005)

Monopole-based universal interaction: V_{MU}

- A quantitative implementation of the basic features
  - Effective tensor force: bare π+ρ meson exchange
    - "Renormalization persistency"
  - Effective central force: Gaussian
    - Phenomenological but supported from empirical interactions

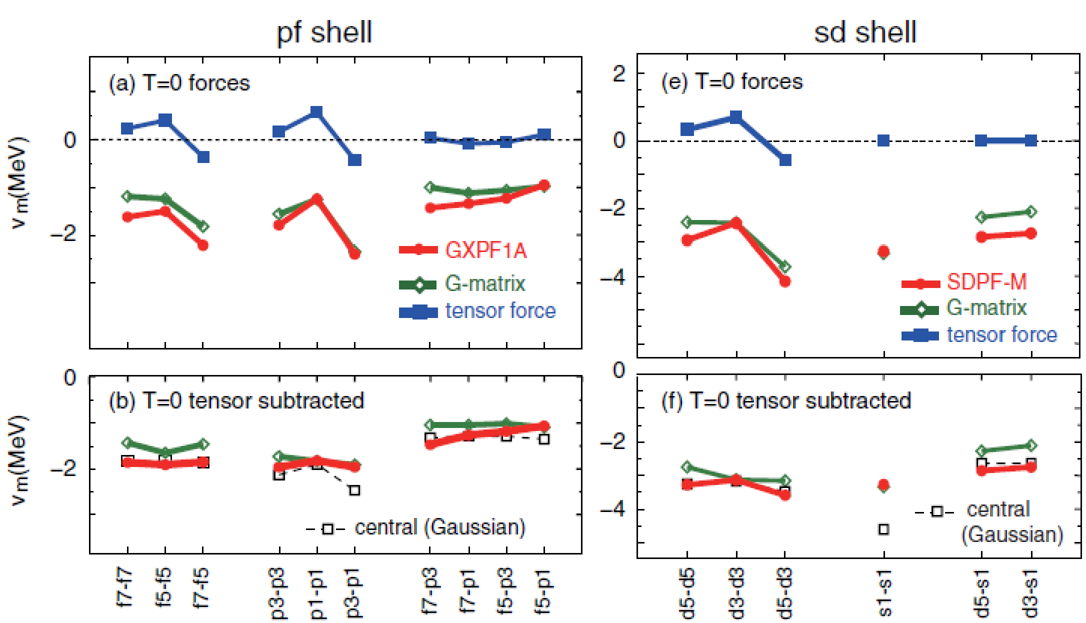

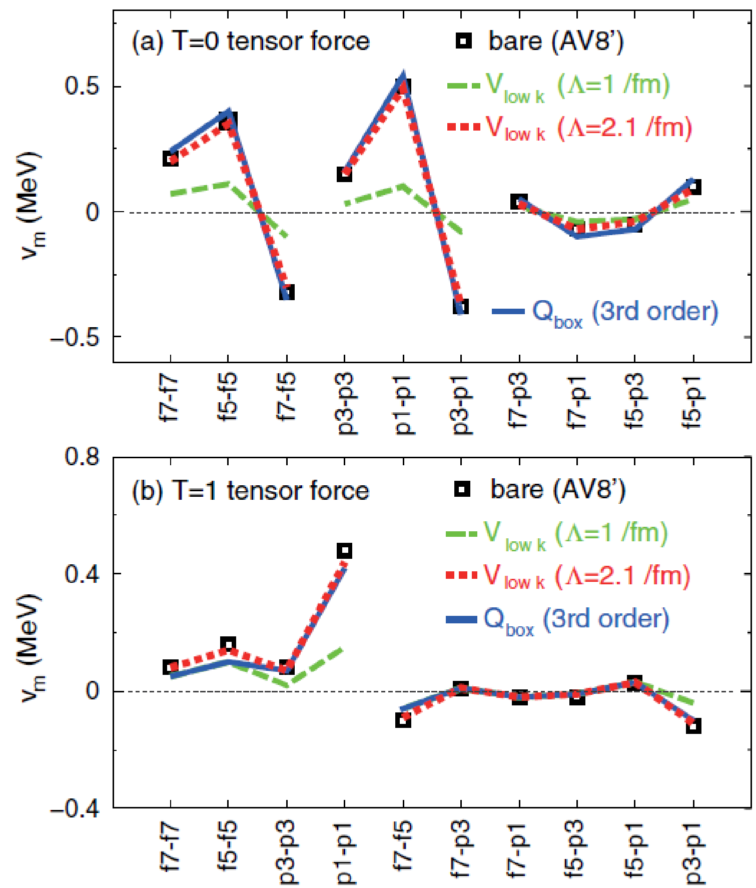

Importance of the tensor force in Sb levels

Pure single-particle picture

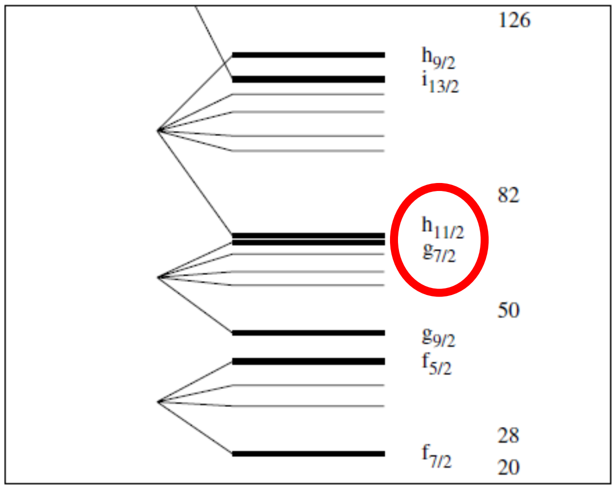

Evolution due to the tensor force

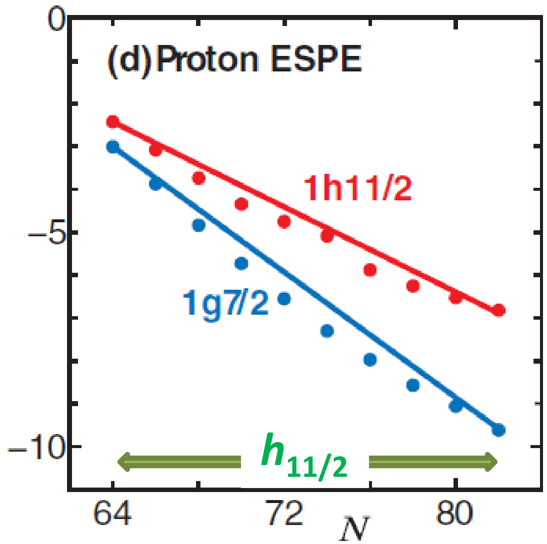

Including correlation

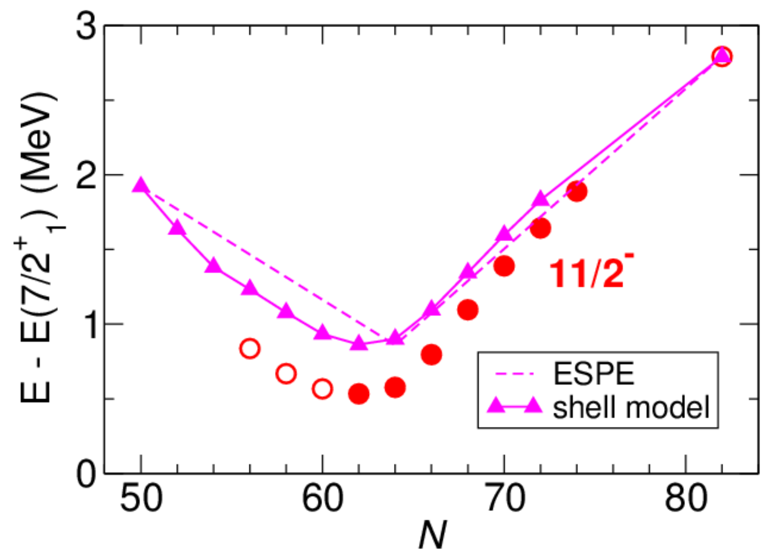

Single-particle strengths

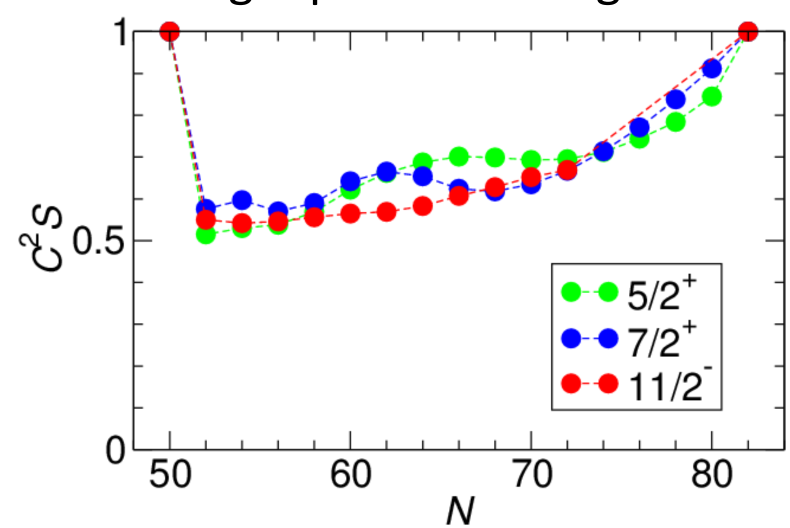

Contents

1. Structure of neutron-rich nuclei in the $N \approx 28$ region
   - V_{MU} interaction for the cross-shell part
   - Reduction of the spin-orbit splitting due to the tensor force
     - Disappearance of the $N=28$ magic number
     - Appearance and possible persistence of the new $N=34$ magic number
2. Monte Carlo shell-model (MCSM) calculations for exotic nuclei
   - Brief overview of MCSM
   - Application to ^{68}Ni: interplay between shell and shape

Neutron-rich *N*≈28 region

Shell evolution of interest:

- Proton side
  - Reduction of spin-orbit splitting
- Neutron side
  - Disappearance of the *N*=28 magic
  - Appearance of the *N*=32, 34 magic

Affecting quadrupole collectivity

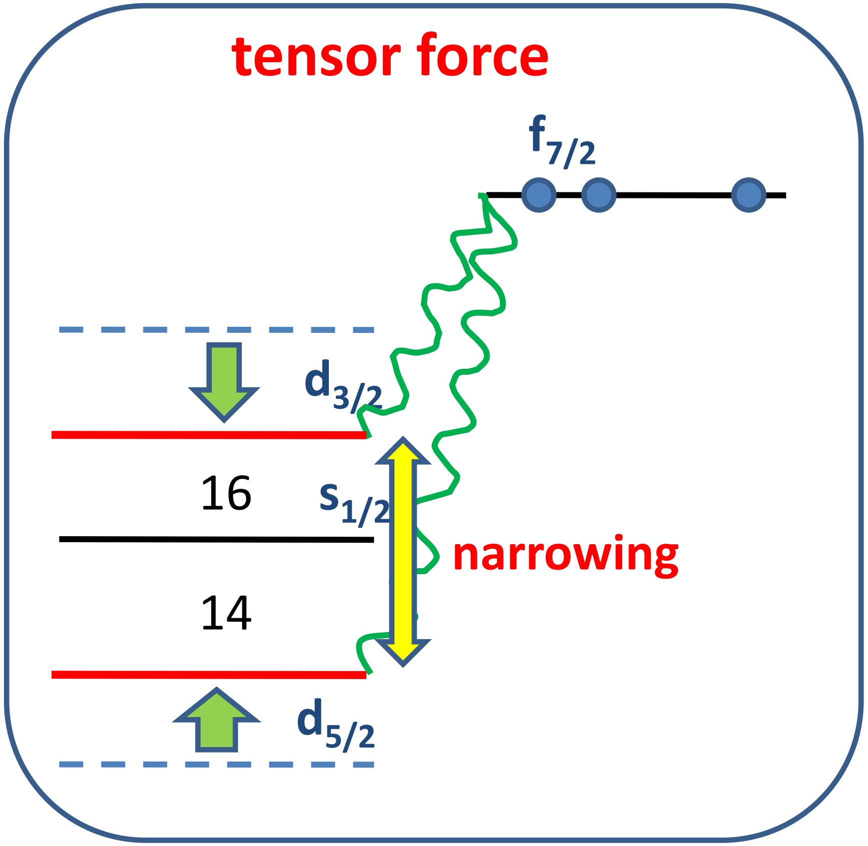

Shell-model calculations

- Model space
  - *sd-pf* shell without excitation across the *N*=20 gap
- Effective interaction
  - Intra-shell: well-tested empirical interactions
    - USD for *sd* and GXPF1B for *pf*
  - Cross-shell: refined V_{MU}
    - tensor: π+ρ
    - spin-orbit: M3Y
    - central: fine-tuned to be close to GXPF1

Central force fitted with six parameters

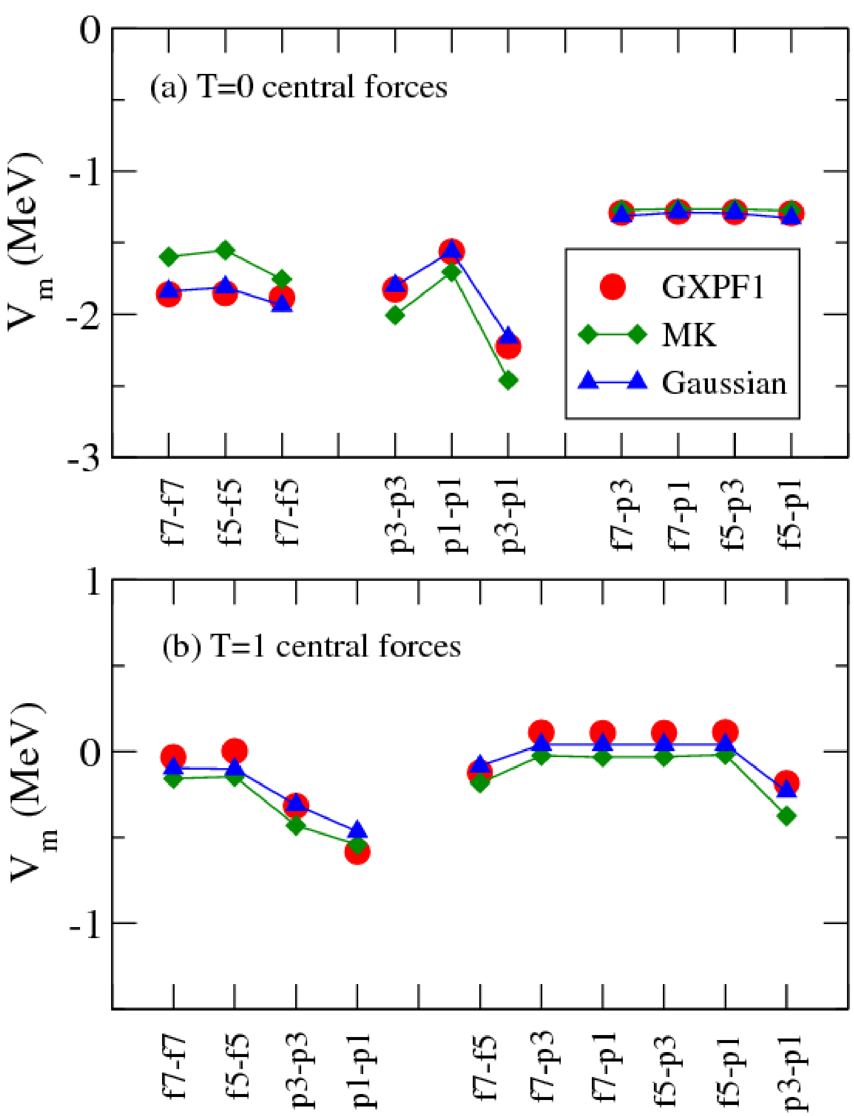

Shell evolution due to V_{MU}

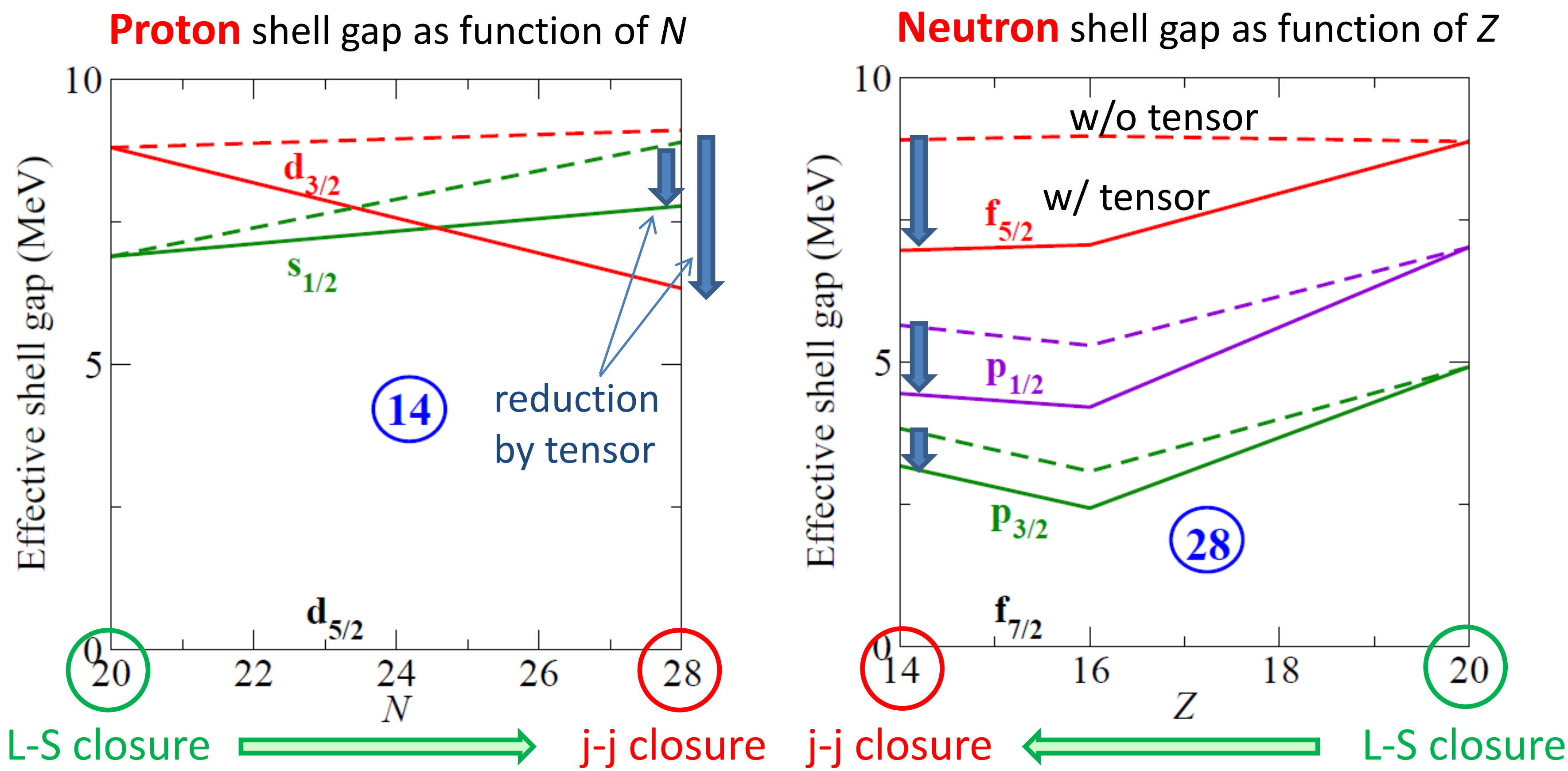

- Tensor force
  - Large effect for doubly j-j closed configurations, such as ^{42}Si and ^{44}S

Probing the spin-orbit splitting in ^{48}Ca

full V_{MU} interaction (w/ tensor) **w/o tensor in the cross shell**

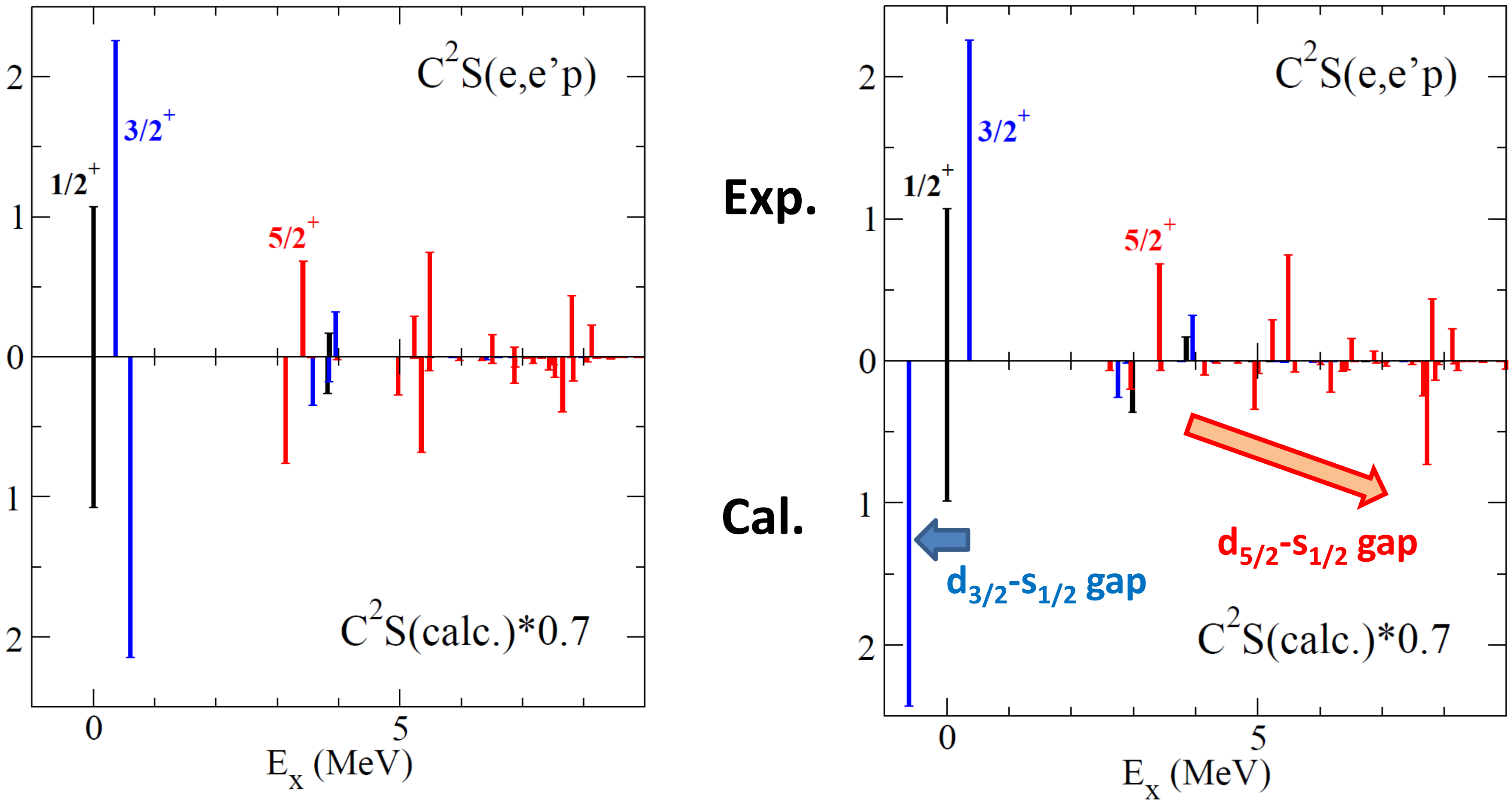

Y. Utsuno et al., Phys. Rev. C 86, 051301(R) (2012).

Occurrence of large deformation in ^{42}Si

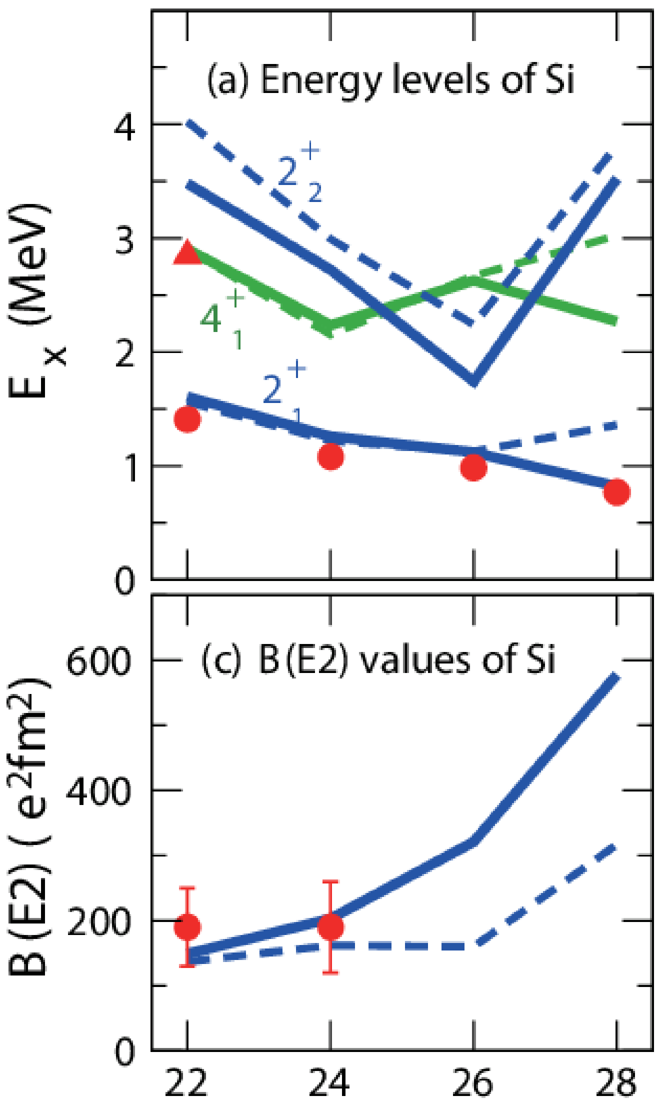

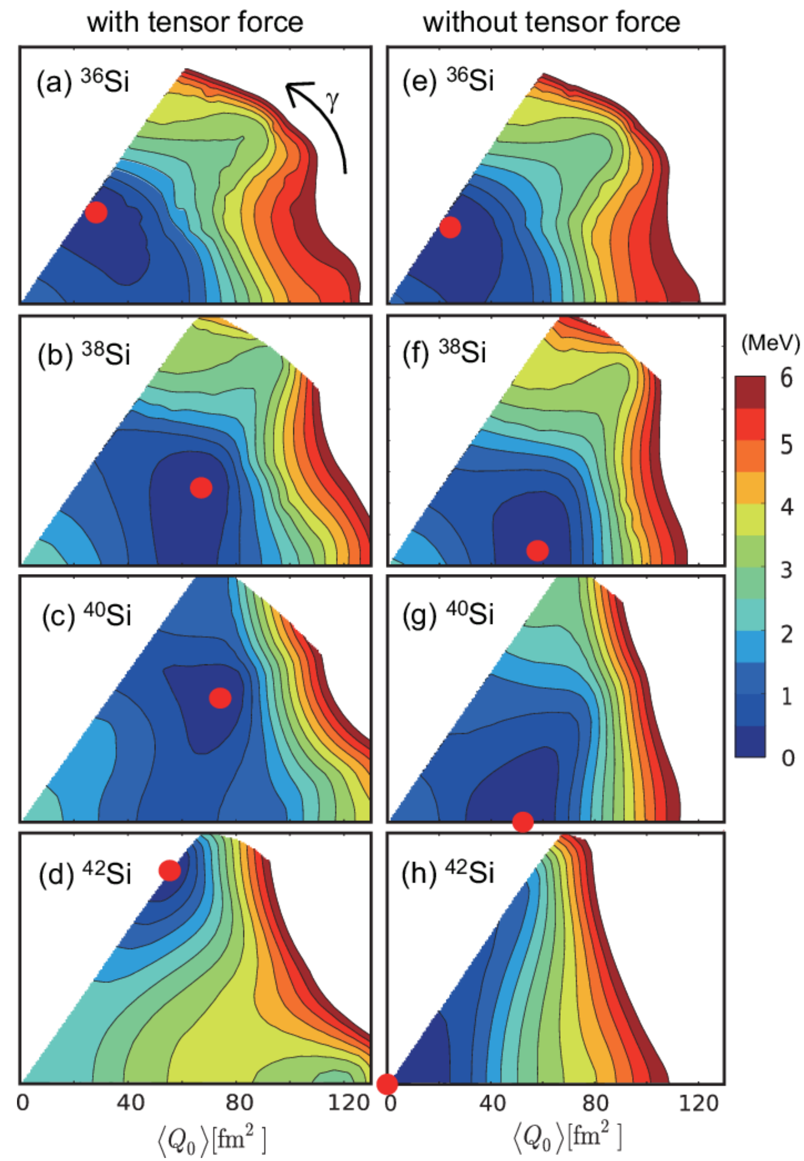

Y. Utsuno et al., Phys. Rev. C 86, 051301(R) (2012).

Tensor-force-driven Jahn-Teller effect

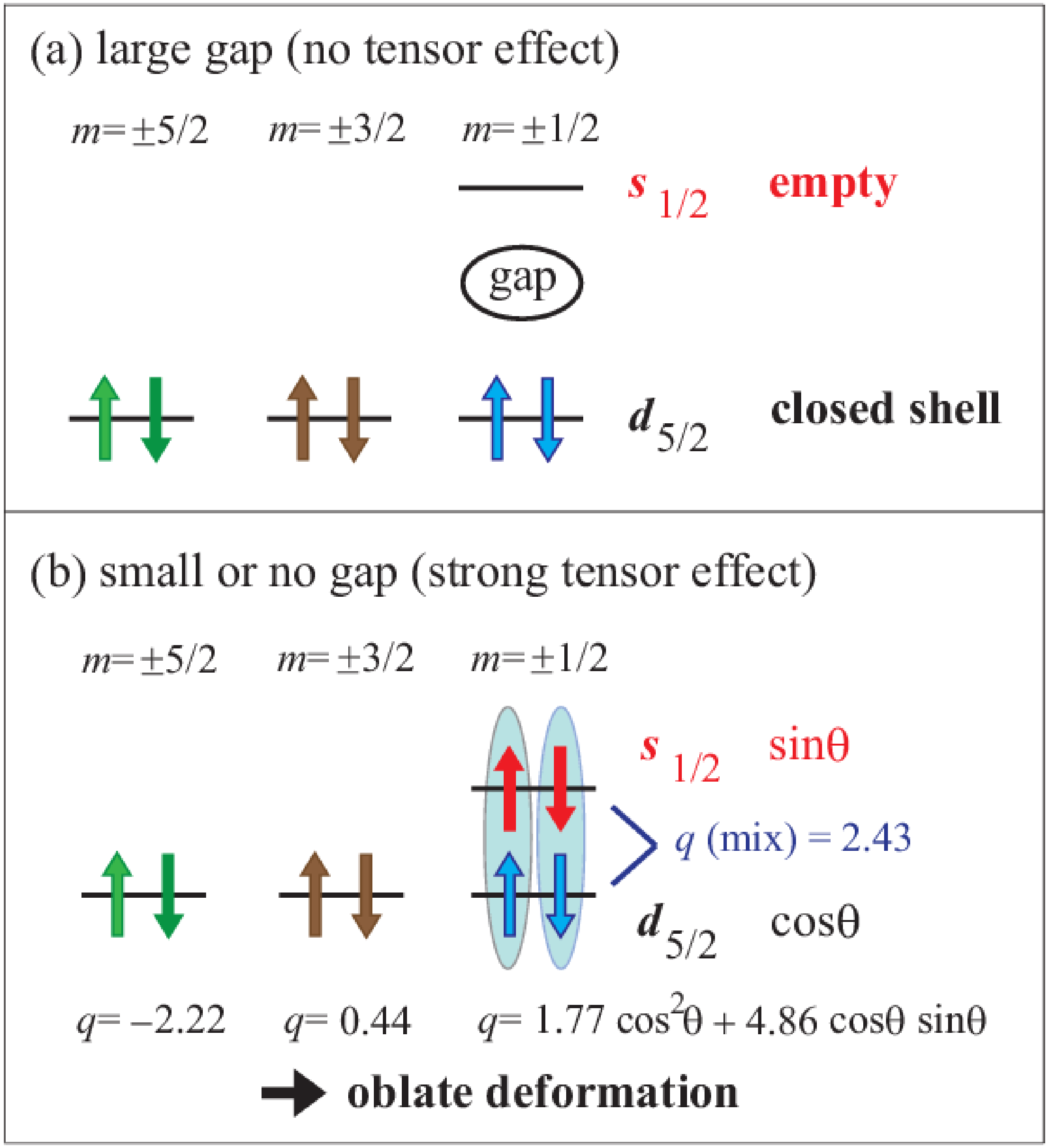

Simple Hamiltonian

H = s.p.e - $Q \cdot Q$

To get lowest energy:

Maximize $|Q|$.

(if s.p.e. is neglected)

Oblate deformation

is favored for Si

to obtain a large $|Q|$.

Evolution of the N=34 magic number

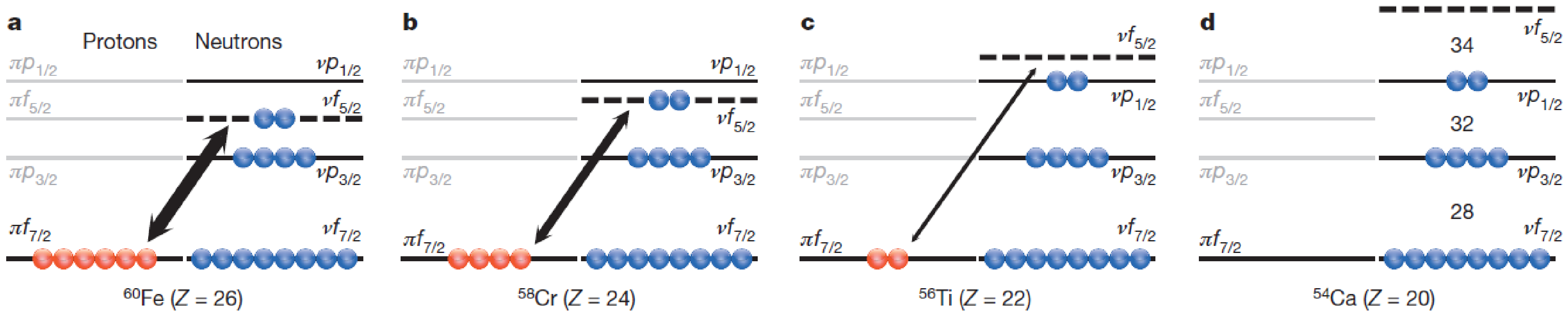

D. Steppenbeck et al., Nature 502, 207 (2013).

- N=34 magic number (at Ca)
  - Predicted by Otsuka et al. in 2001, but no experimental signs were found before
- Direct measurement of 2^+_1 for ^{54}Ca at RIBF
  - Establishing magicity (Steppenbeck et al., 2013 and talk on Friday)
- Very localized magic number
  - Sharp lowering of $f_{5/2}$ due to central and tensor

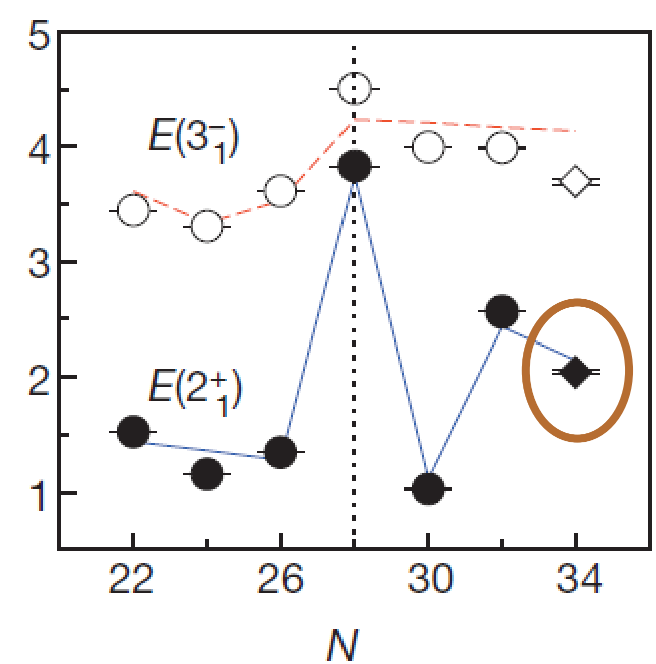

How large is the *N*=34 gap at Ca?

- GXPF1B (Honma, 2008: 3.21 MeV gap) vs. GXPF1Br (2.66 MeV gap)
  – Systematic improvement with GXPF1Br (^{51}Ca: suggested by Rejmund et al.)

    ~2.5 MeV gap is established.

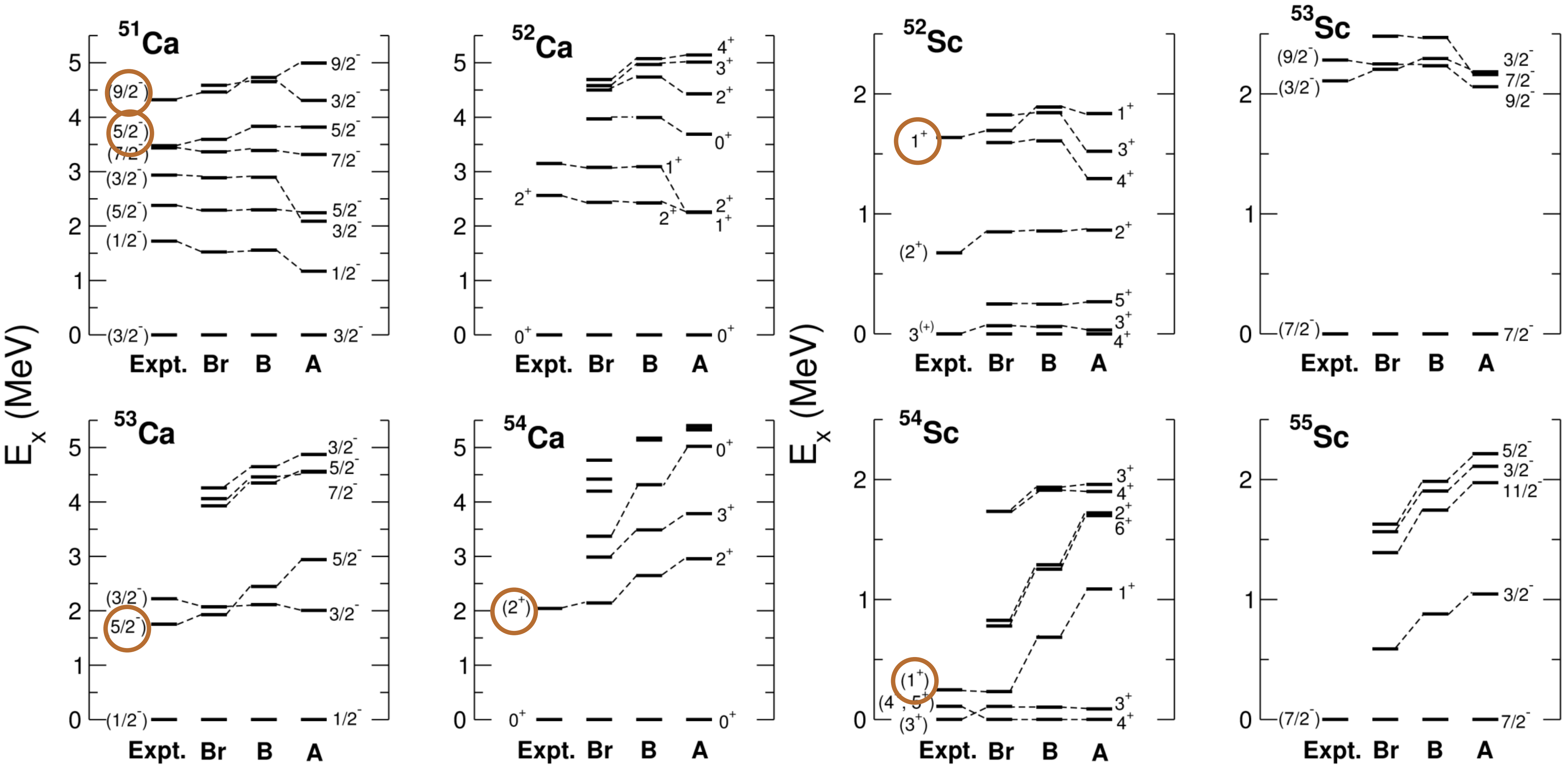

Separation energies of Ca isotopes

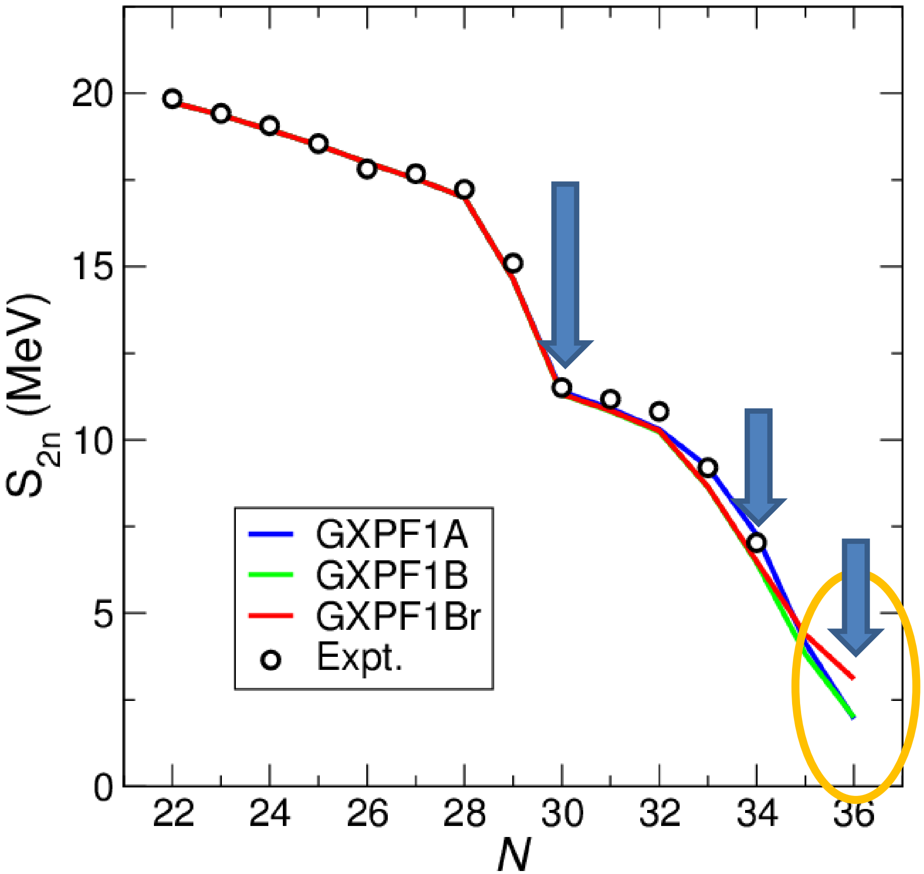

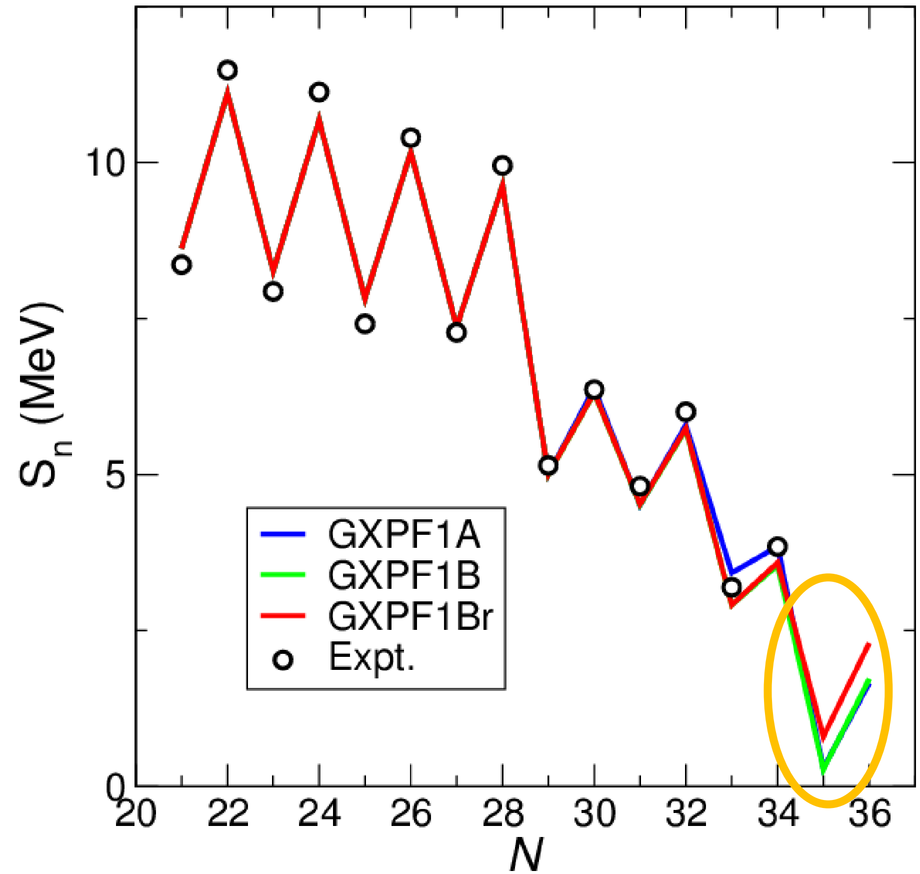

- Prediction with GXPF1Br
  - Drop of separation energies beyond *N*=34 is predicted due to the *N*=34 gap, but it is not as pronounced as that of GXPF1A or GXPF1B.

N=34 gap: Persist or diminish in lower *Z*?

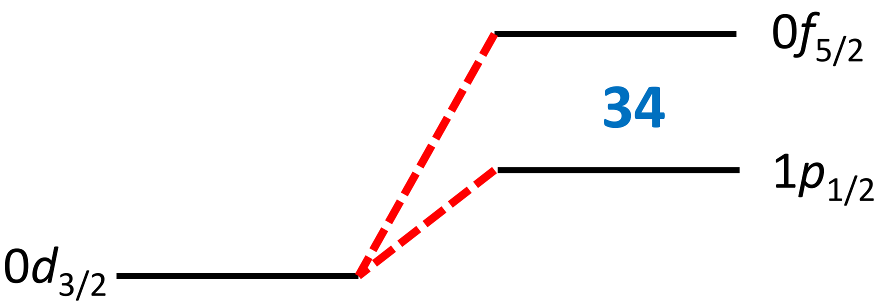

V_{MU} (with spin-orbit force)

	Central	SO	Tensor
*d*3-*f*5	-1.184	+0.041	+0.278
*d*3-*p*1	-0.706	+0.045	+0.091
diff.	-0.478	-0.004	+0.187

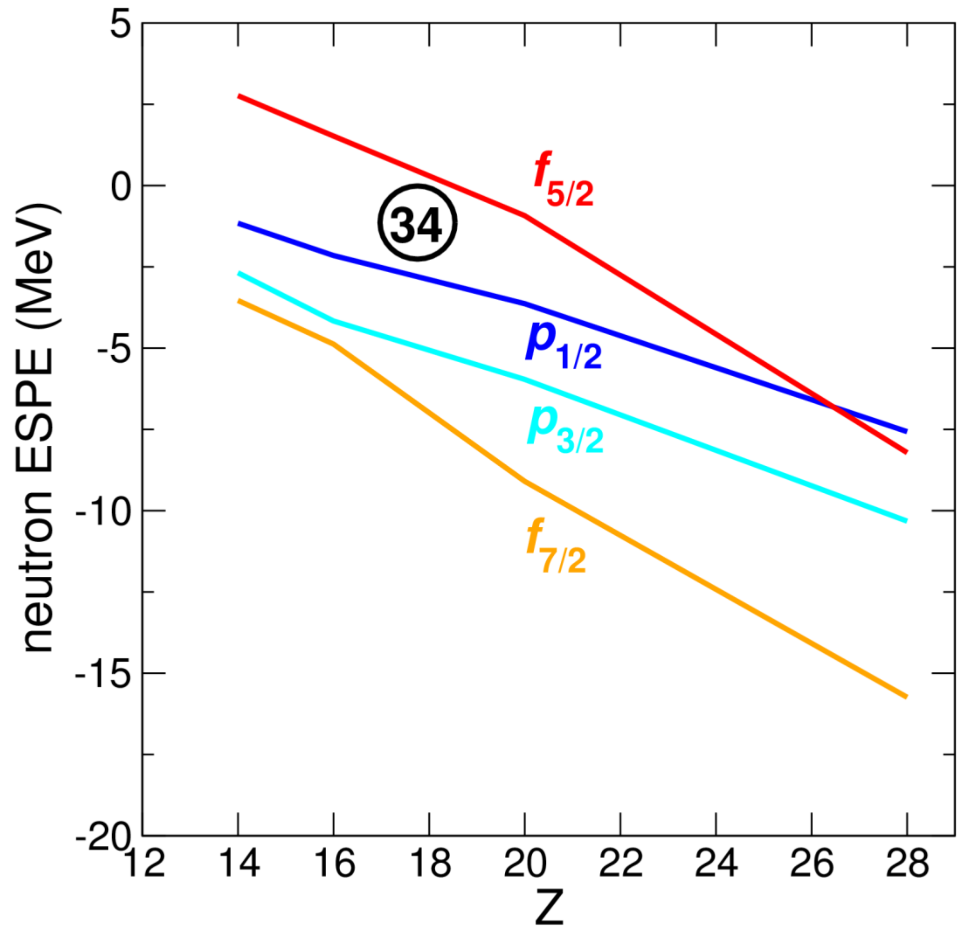

Some enhancement of the *N*=34 gap for lower *Z*

Possible widening of the *N*=34 gap for lower *Z*

- Spectroscopic factors available
  - Along the *N*=20 core, but not the *N*=34 core
  - However, according to shell evolution due to the monopole interaction, the change of the shell gap is irrelevant to the neutron core assumed.

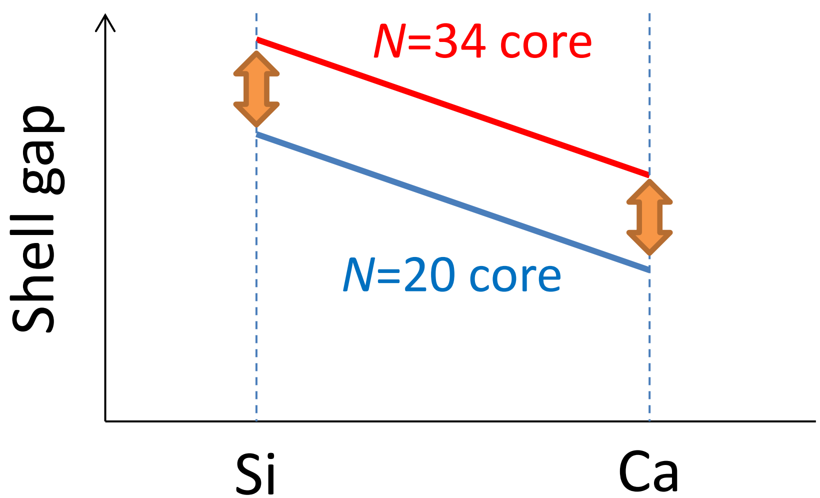

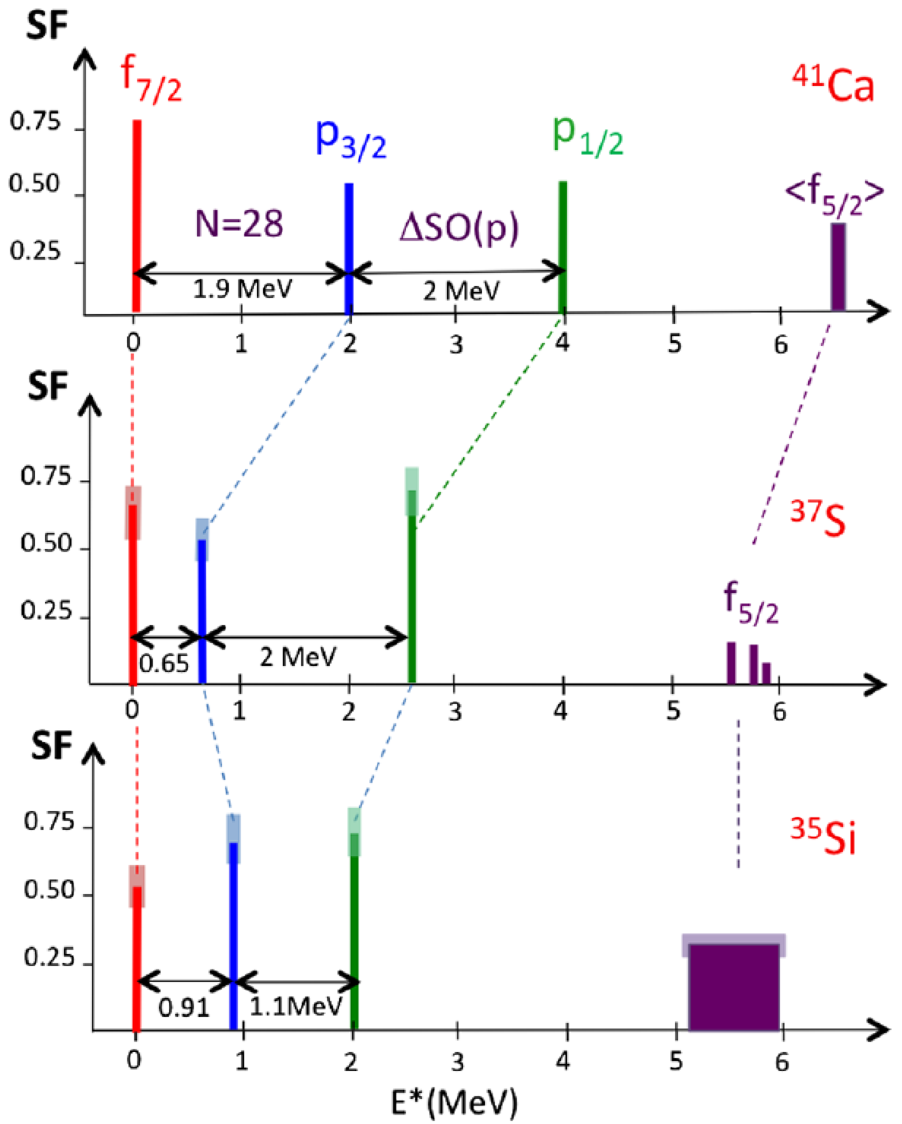

G. Burgunder et al., Phys. Rev. Lett. 112, 042502 (2014).

2^+ levels: comparison between π(*pf*) and π(*sd*)

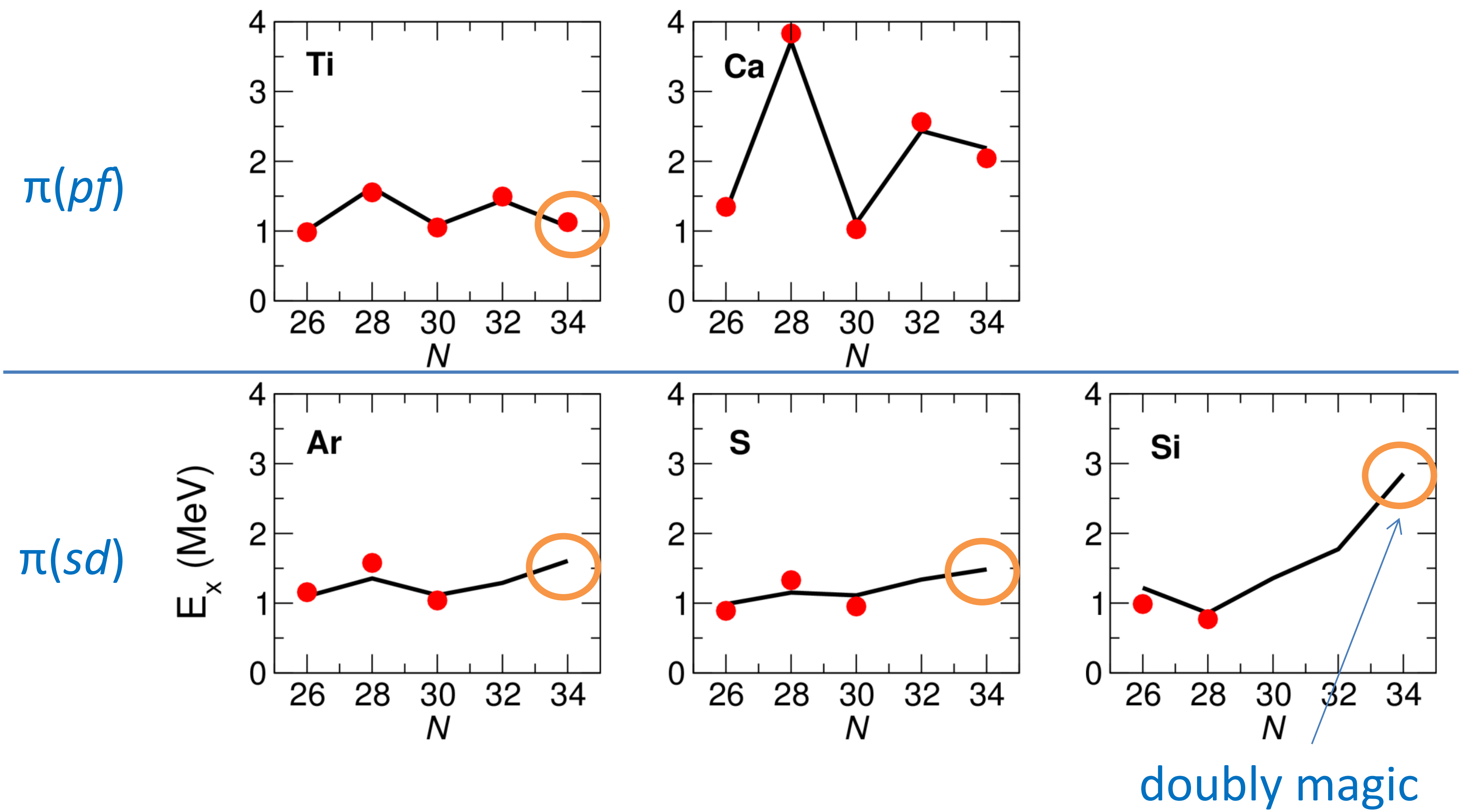

Monte Carlo shell-model calculation

Basic idea

- Reducing the size of the Hamiltonian matrix
  - Possible if one can choose a set of “efficient” basis states

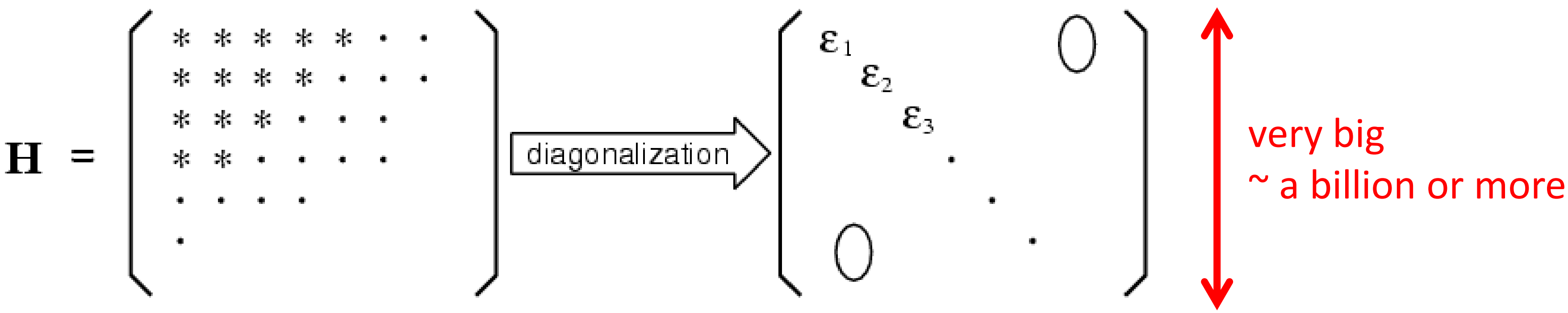

Conventional Shell Model
all Slater determinants

spherical-basis representation

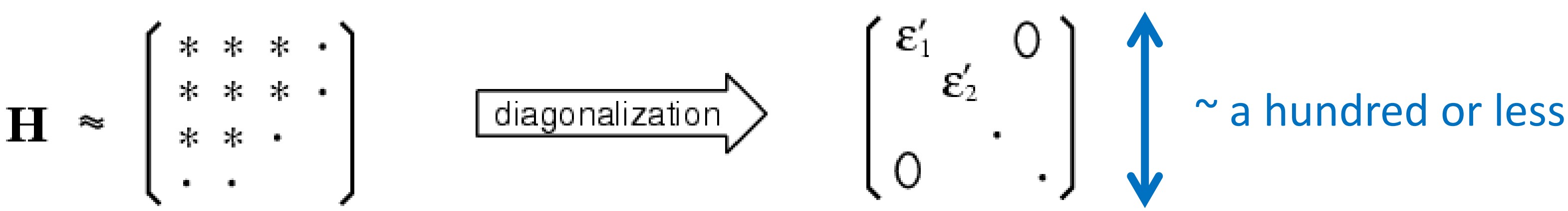

Monte Carlo Shell Model
bases important for a specific eigenstate

“selected”-basis representation

T. Otsuka, M. Honma, T. Mizusaki, N. Shimizu, and Y. Utsuno, Prog. Part. Nucl. Phys. 47, 319 (2001).

Spherical vs. deformed basis state

- Spherical basis state (Slater det.)

$$c_{p(1)}{}^{\dagger} \cdots c_{p(N_p\,(p))}{}^{\dagger} c_{n(1)}{}^{\dagger} \cdots c_{n(N_p\,(n))}{}^{\dagger} |\mathrm{core}\rangle$$

  – Each single-particle state created by $c_{p(i)}{}^{\dagger}$ or $c_{n(i)}{}^{\dagger}$ has a good *j* and *m*.

- Deformed basis state (Slater det.)

$$a_{p(1)}{}^{\dagger} \cdots a_{p(N_p\,(p))}{}^{\dagger} a_{n(1)}{}^{\dagger} \cdots a_{n(N_p\,(n))}{}^{\dagger} |\mathrm{core}\rangle$$

  – Each single-particle state created by $a_{p(i)}{}^{\dagger}$ or $a_{n(i)}{}^{\dagger}$ does not necessarily have a good *j* or a good *m*.

  – Mixing among different spherical states is characterized by a matrix D:

$$a_i{}^{\dagger} = D_{1i} c_1{}^{\dagger} + D_{2i} c_2{}^{\dagger} + \cdots + D_{N_p i} c_{N_p}{}^{\dagger}$$

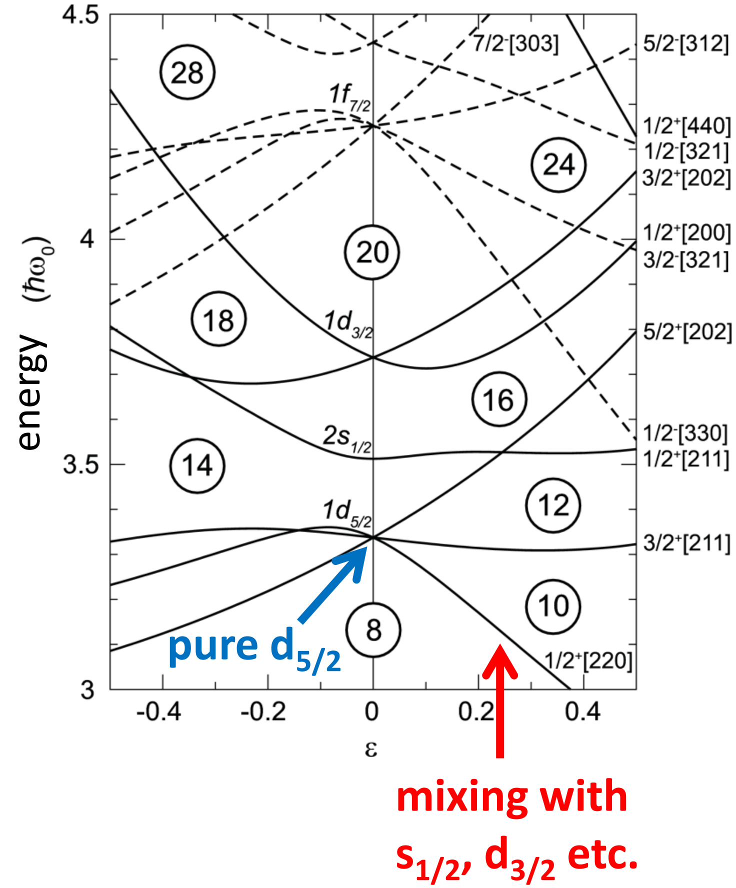

MCSM wave function

- Superposition of deformed Slater determinants with symmetry restoration

MCSM basis dimension ≈ 100

$$|\Psi^{IM\pi}(N_b)\rangle = \underbrace{\sum_{d=1}^{N_b} f^{(d)}}_{\text{superposition}} \underbrace{\sum_{K=-I}^{I} g_K^{(d)} \; \hat{P}^{\pi} \, \hat{P}^{I}_{MK}}_{\text{Projection onto good } I,\, M,\, \pi} \underbrace{|\Phi(D^{(d)})\rangle}_{\text{deformed basis state}}$$

where $|\Phi\left(D^{(d)}\right)\rangle = \prod_i a\left(D^{(d)}\right)_i^{\dagger} |\mathrm{core}\rangle$ and $a\left(D^{(d)}\right)_i^{\dagger} = \sum_l D_{li}^{(d)} c_l^{\dagger}$

- The energy of the state is determined by a set of $D^{(d)}$ (d=1, …, N_b): $\left\{D^{(1)}, \dots, D^{(N_b)}\right\} \xrightarrow{\text{yields}} E^{(N_b)}$. f and g_K are automatically determined by diagonalizing H.
- Ideally, the matrices $D^{(d)}$ are determined from the variational principle. But its practical implementation is not easy.

Sequential optimization

- In most cases, we adopt a sequential optimization scheme for $D^{(k)}$ (k=1, …, N_b), i.e., optimization carried out in the order $D^{(1)}$, $D^{(2)}$, …
  - The first basis state is determined with the variation after angular-momentum projection method.
  - In optimizing the second basis characterized by $D^{(2)}$, the first basis is fixed by the above-mentioned basis. Only $D^{(2)}$ is varied to obtain the energy as low as possible.
  - Similarly, in optimizing the k-th basis characterized by $D^{(k)}$, the basis states already taken (i.e., $D^{(1)}$, $D^{(2)}$, …, $D^{(k\text{-}1)}$) are fixed. Only $D^{(k)}$ is varied to obtain the energy as low as possible.
- The resulting energy $E^{(Nb)}$ decreases with increasing N_b.

Stochastic or deterministic optimization

- We choose either of the followings:
  1. Stochastic optimization (adopted by the original MCSM)
     - Stochastic variation following a Monte Carlo sampling
     - If energy is lowered, this variation is adopted. If not, rejected.
  2. Deterministic optimization (adopted by recent calculations)
     - Calculating the conjugate gradient (CG) vector on the energy surface
     - Follow the direction of the CG vector until the minimum along the line.

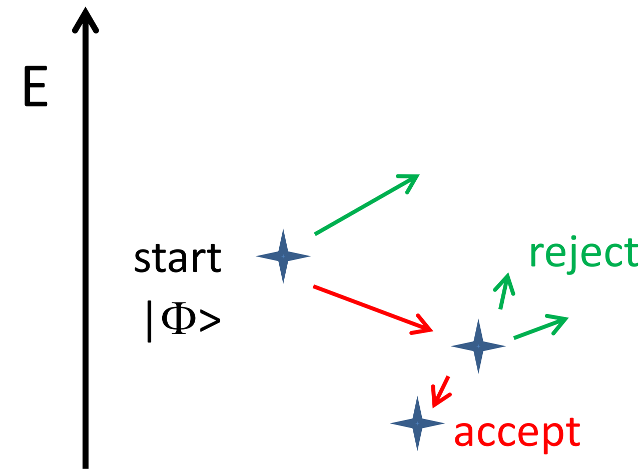

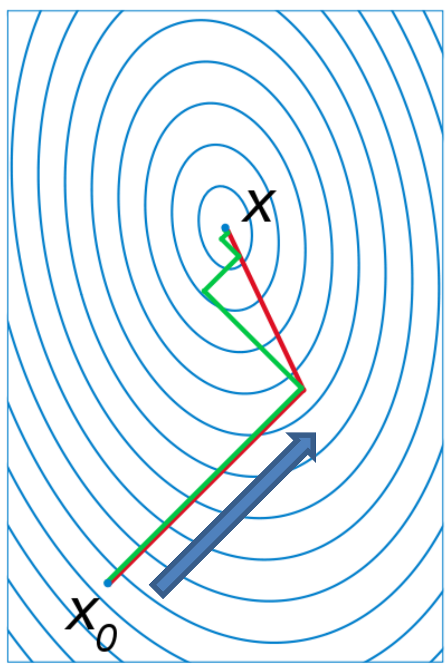

Efficiency of parallel computing in MCSM

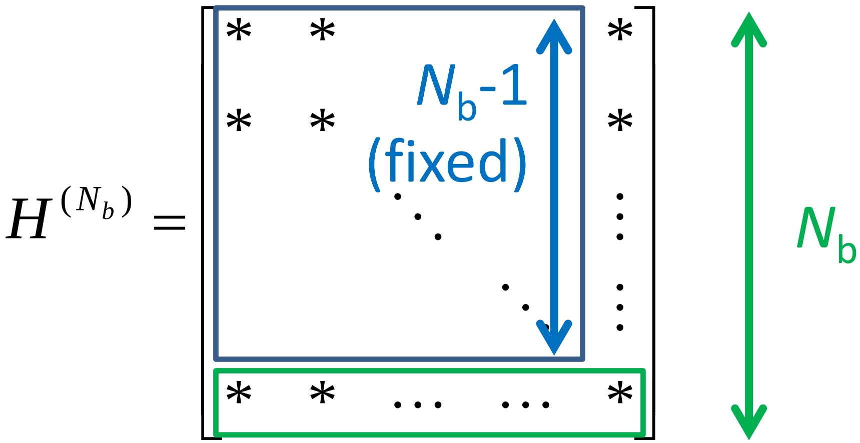

N_b projected matrix elements are calculated at the same time.

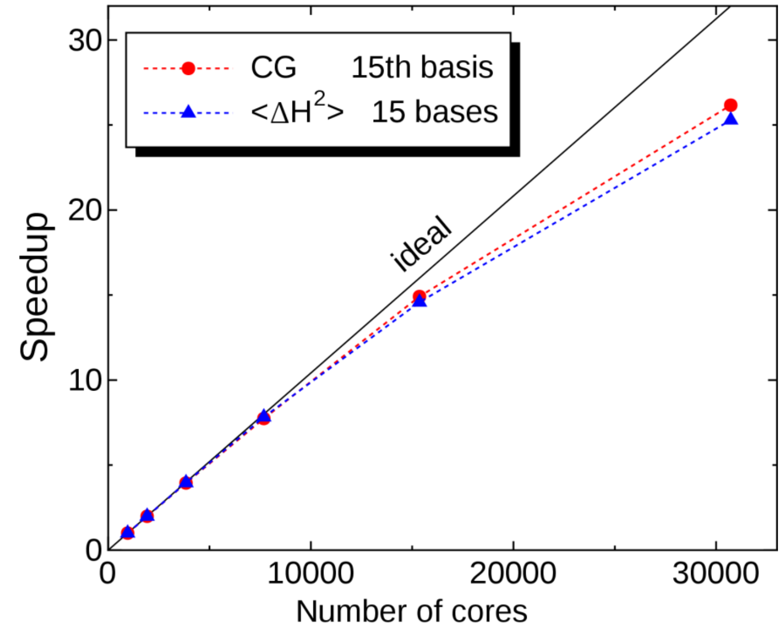

- Calculating one projected matrix element requires ten thousands of unprojected matrix elements because of three-dimensional integral (along the Euler angles):

  # matrix elements = $2 \times N_{meshz}{}^2 \times N_{meshy} \times N_b \approx 10^6 >>$ # cores

  high parallel efficiency

Demonstrating the efficiency of MCSM

- Example: ^{56}Ni in the pf shell with *M*-scheme dimension about 10^9

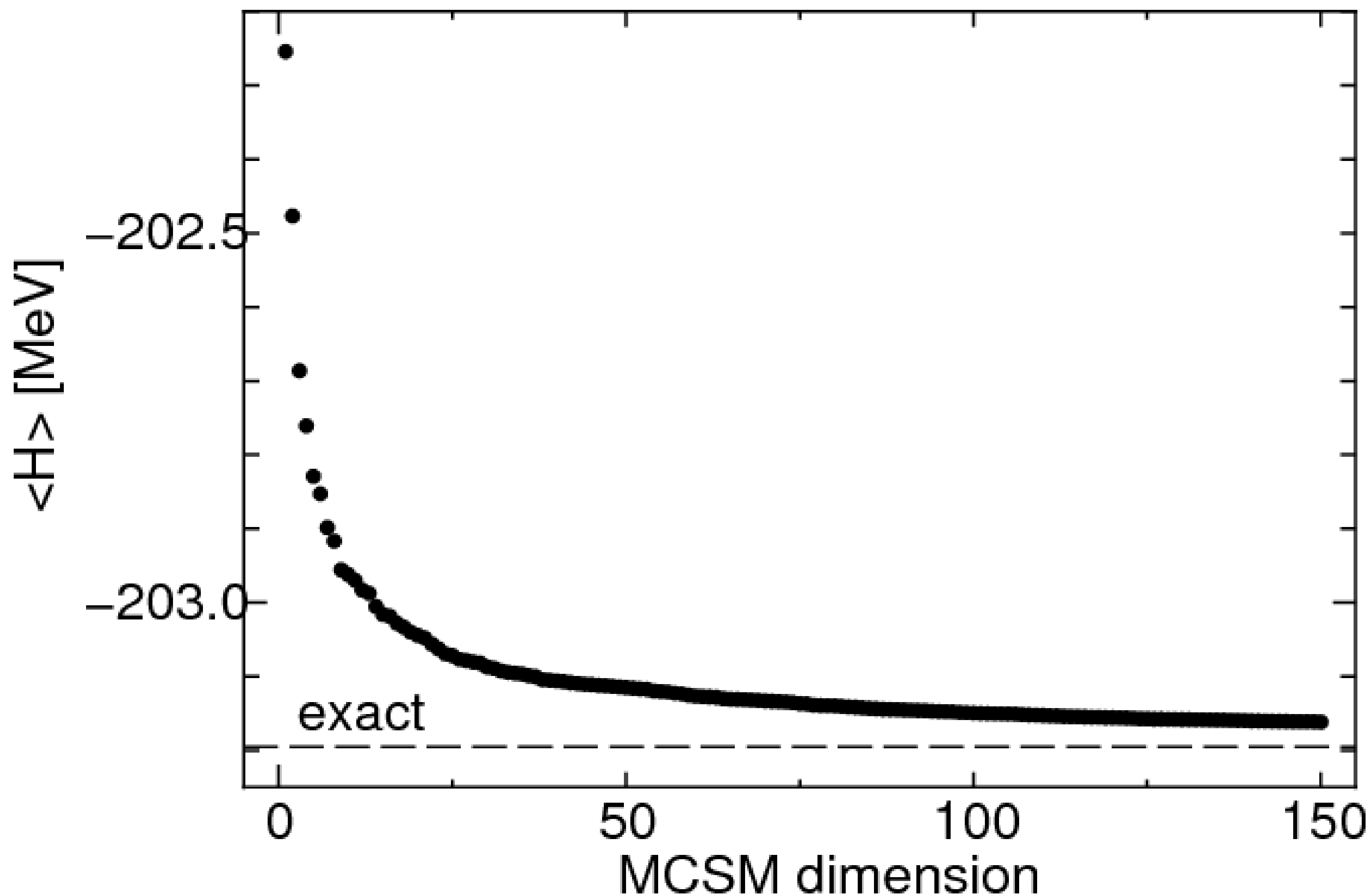

Estimating the exact energy: extrapolation

- Difficult to estimate the exact energy from the dimensional plot
- Utilizing energy variance $\langle H^2\rangle - \langle H\rangle^2$
  - Introduced to the Lanczos diagonalization by Mizusaki and Imada
  - The variance of an eigenstate vanishes. Extrapolation thus works well.

Energy as a function of **variance**

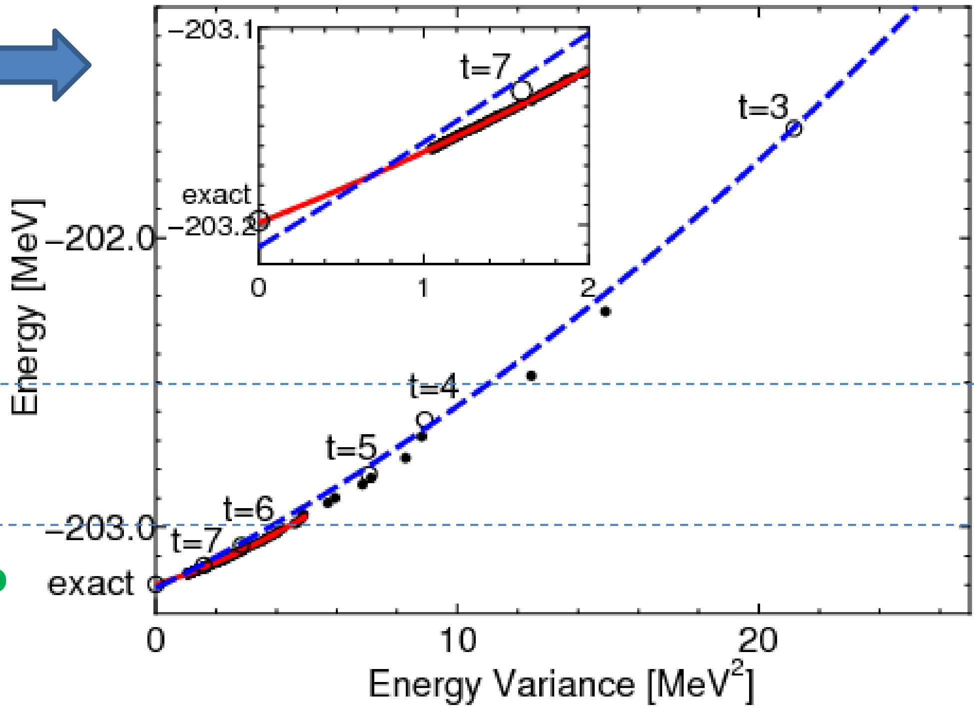

Energy as a function of **dimension**

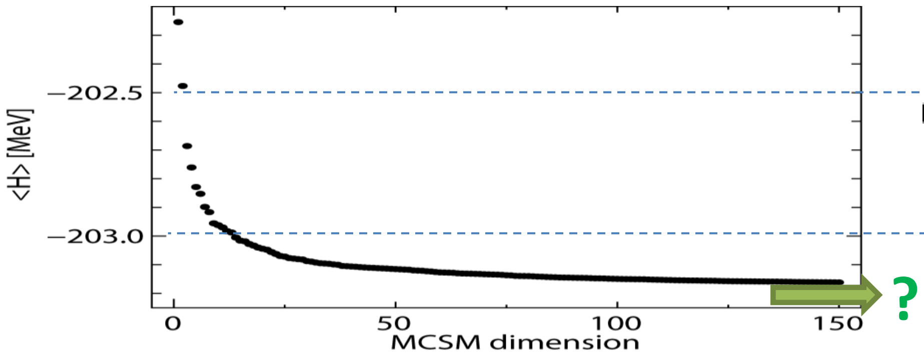

N. Shimizu et al., Phys. Rev. C 82, 061305(R) (2010).

Extrapolated energies for different methods

- Comparison between stochastic and deterministic variations
  - Example: ^{64}Ge in the pf-$g_{9/2}$ shell (10^{14} dimension: beyond current limit)
  - The deterministic way (MCSM+CG) gives lower energies for given dimensions, but the extrapolated energies are almost the same.

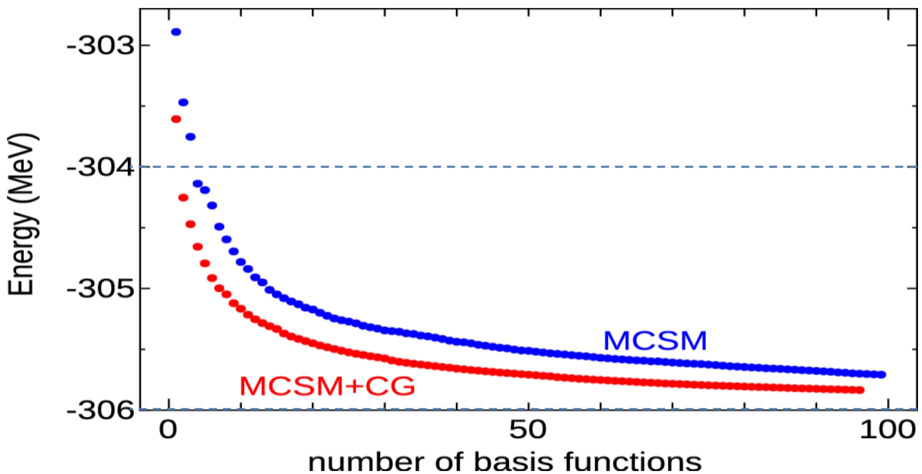

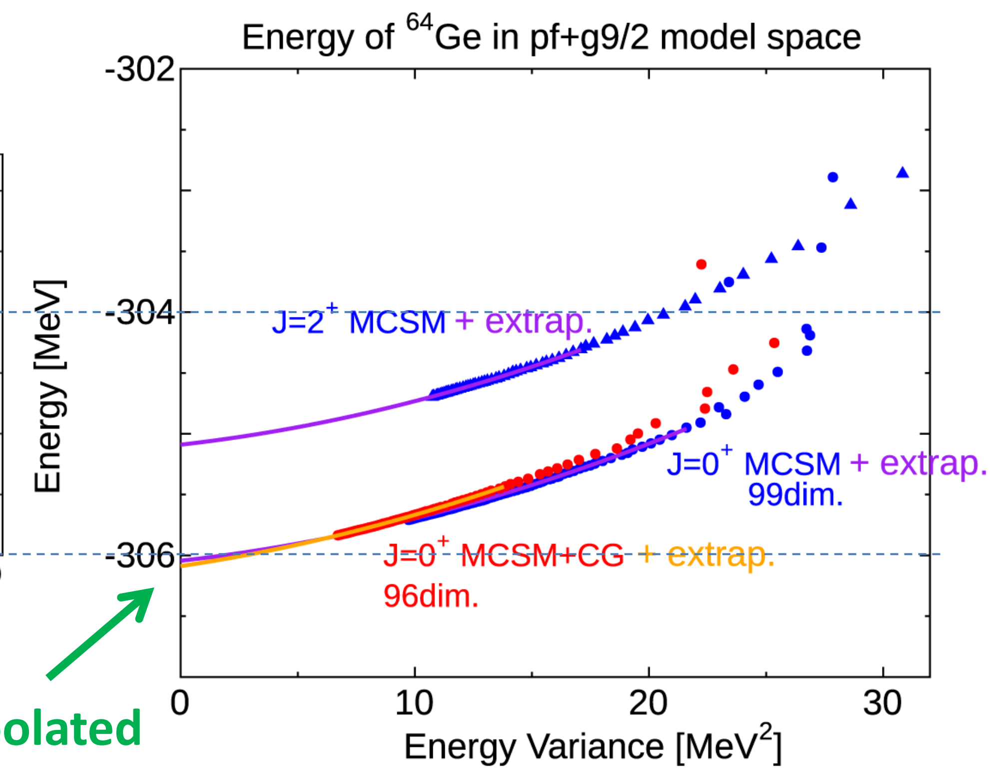

Courtesy of N. Shimizu

extrapolated energy

Application to exotic nuclei: ^{68}Ni

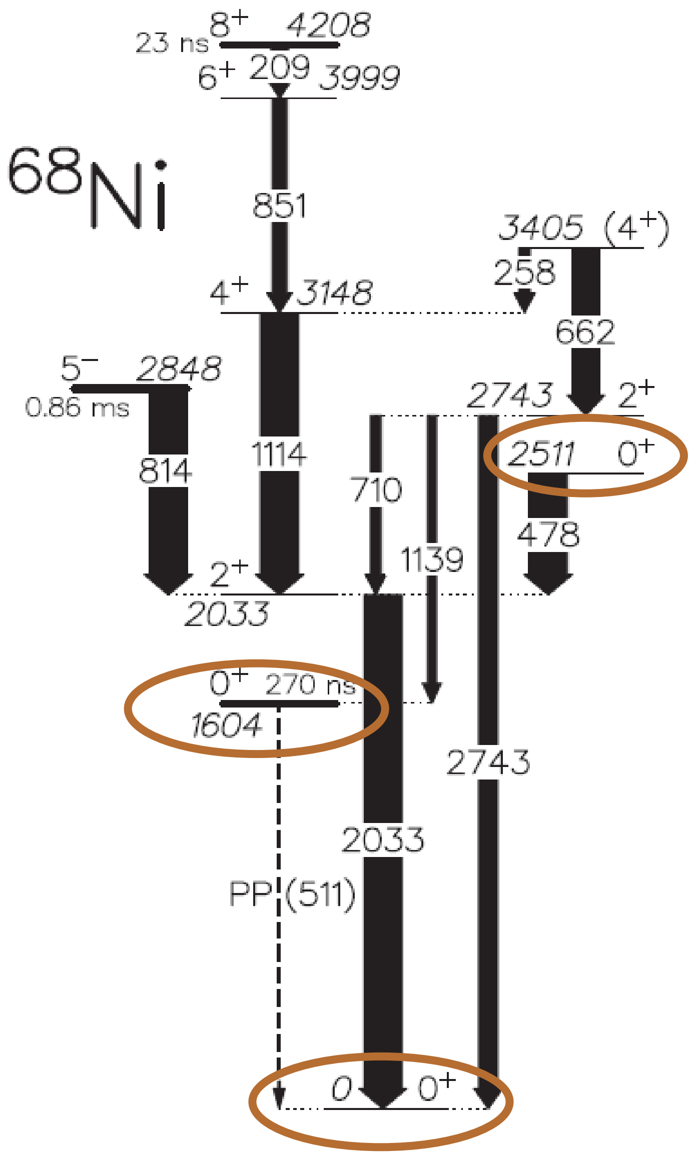

- Unusual level structure
  - Three low-lying 0^+
  - Nature of those states?

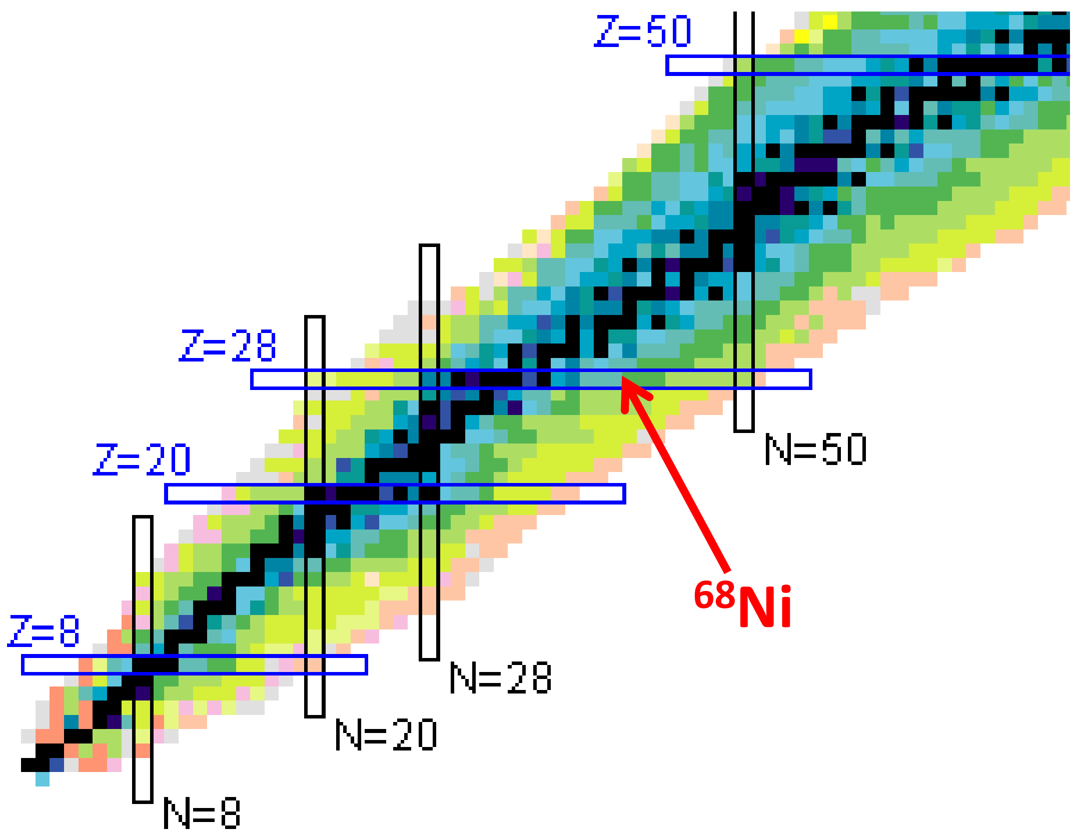

Triple shape coexistence in ^{186}Pb

- A similar situation known for $^{186,188}Pb$
  - Interpreted as spherical-oblate-prolate shape coexistence

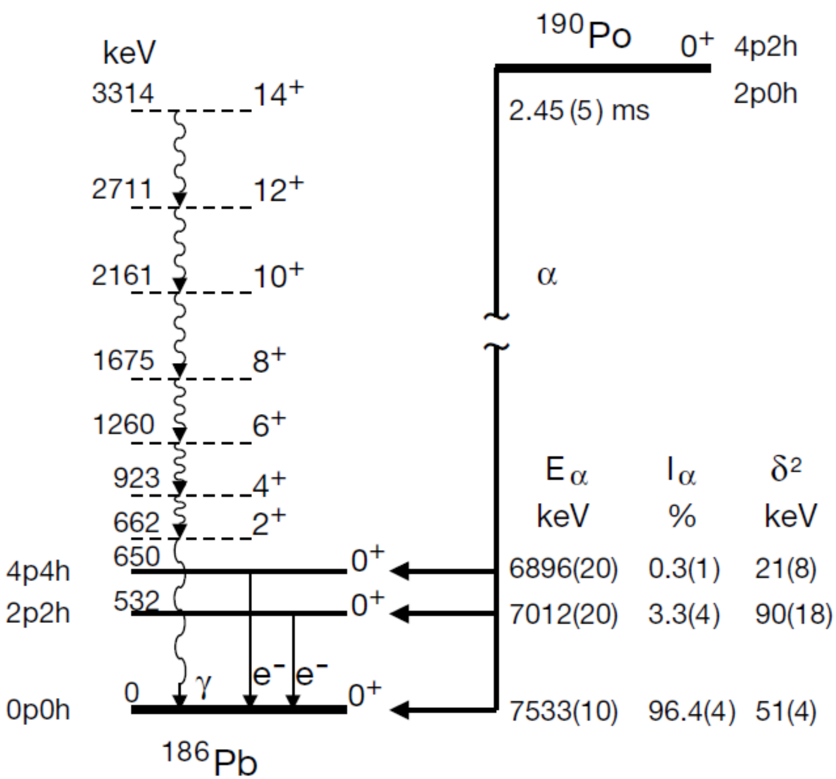

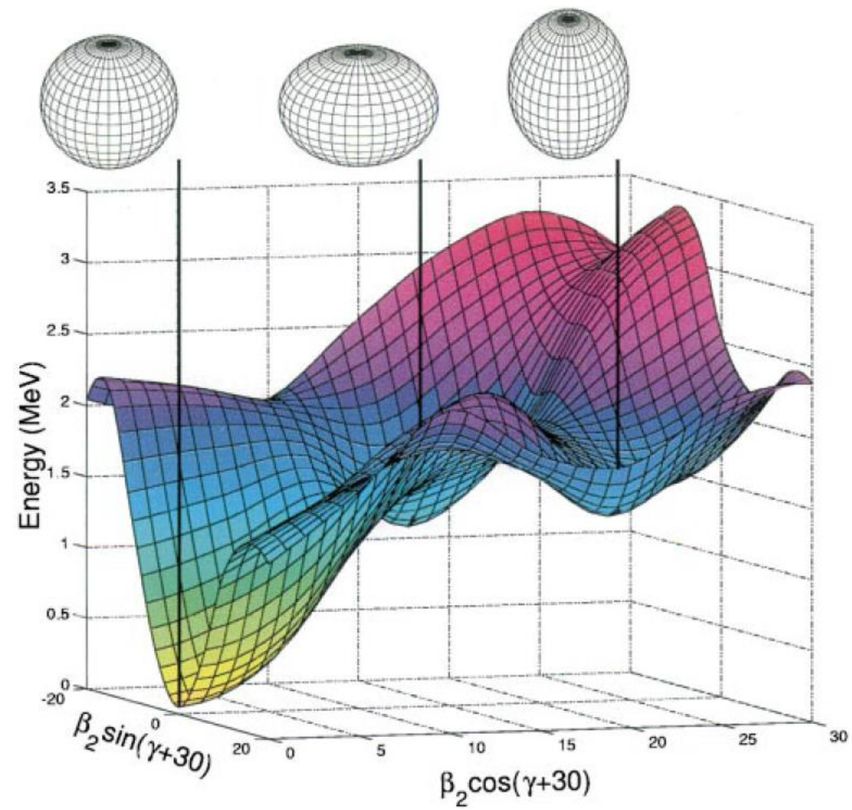

A. N. Andreyev et al., Nature 405, 430 (2000).

Shell-model calculations in a small space

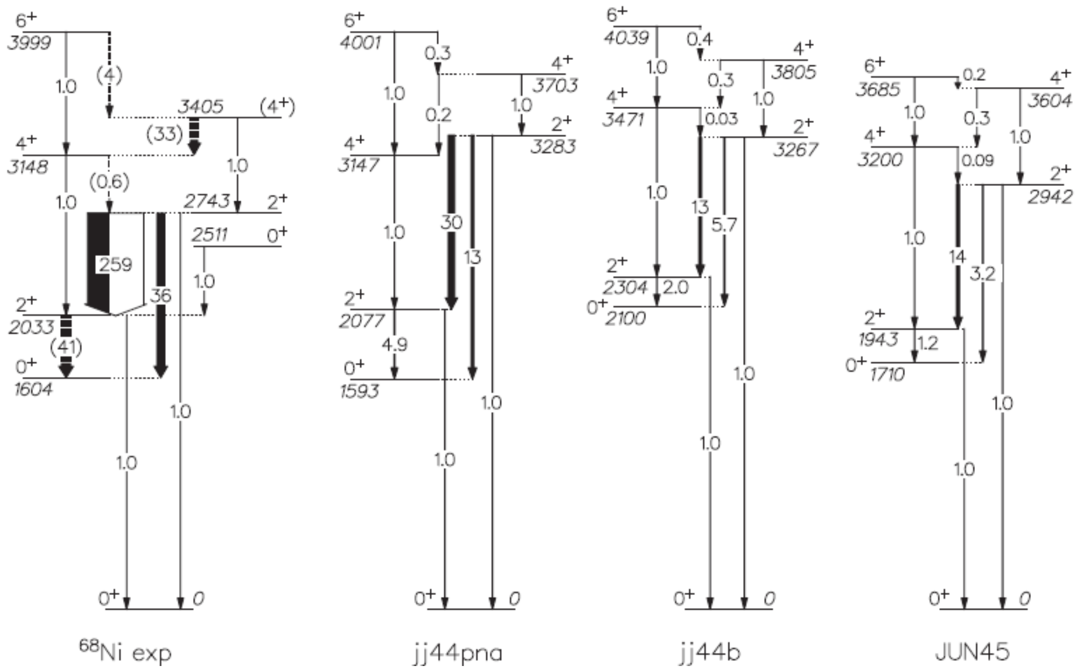

- Missing 0^+_3
  - Due to small model space
  - Very large-scale calculation is needed to describe.

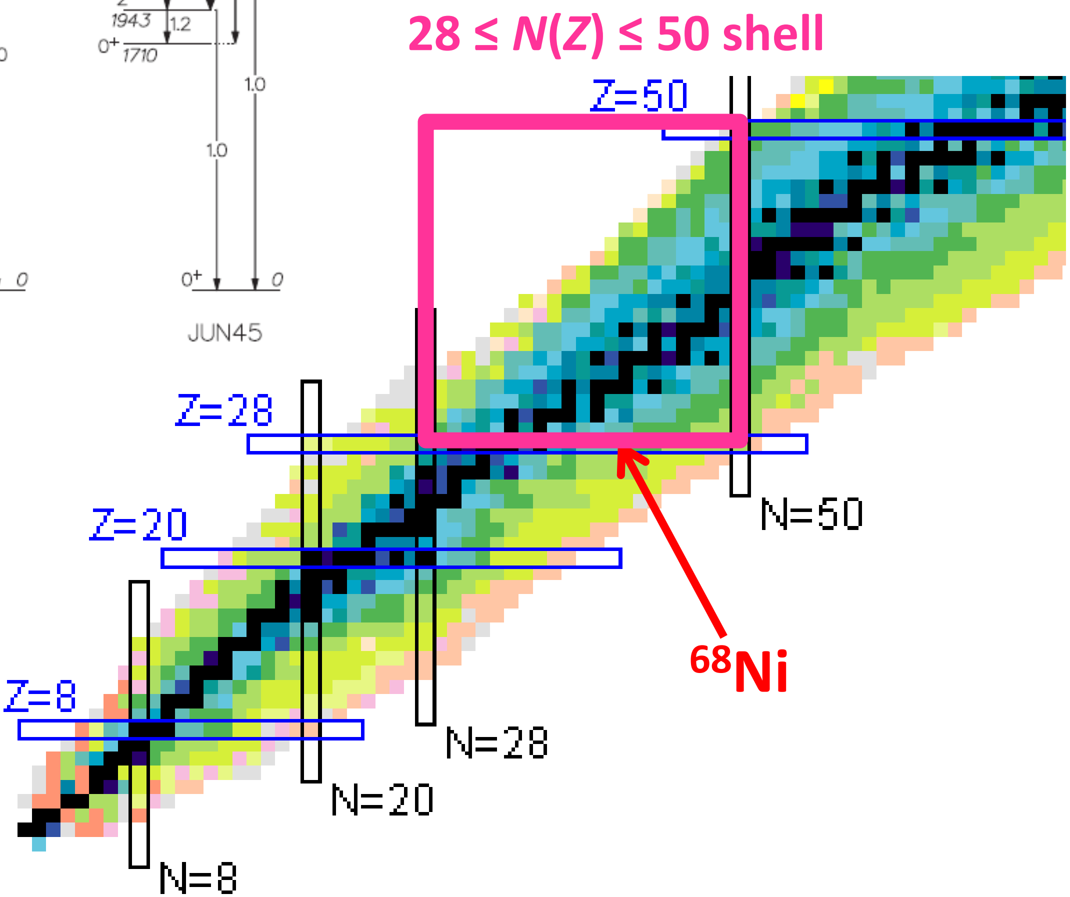

Shell-model calculation in a large space

- Shell-model calculation in the $20 \leq N(Z) \leq 56$ shell
  - $f_{7/2}$ and $d_{5/2}$ orbits are included in addition to the $28 \leq N(Z) \leq 50$ space.
    - 10^{15} M-scheme dimension: beyond current limit
    - A reasonable truncation (up to ~10^{10} dimension) to this space works well (Lenzi et al., 2010).
    - Here we apply MCSM to systematic calculations for Ni isotopes.

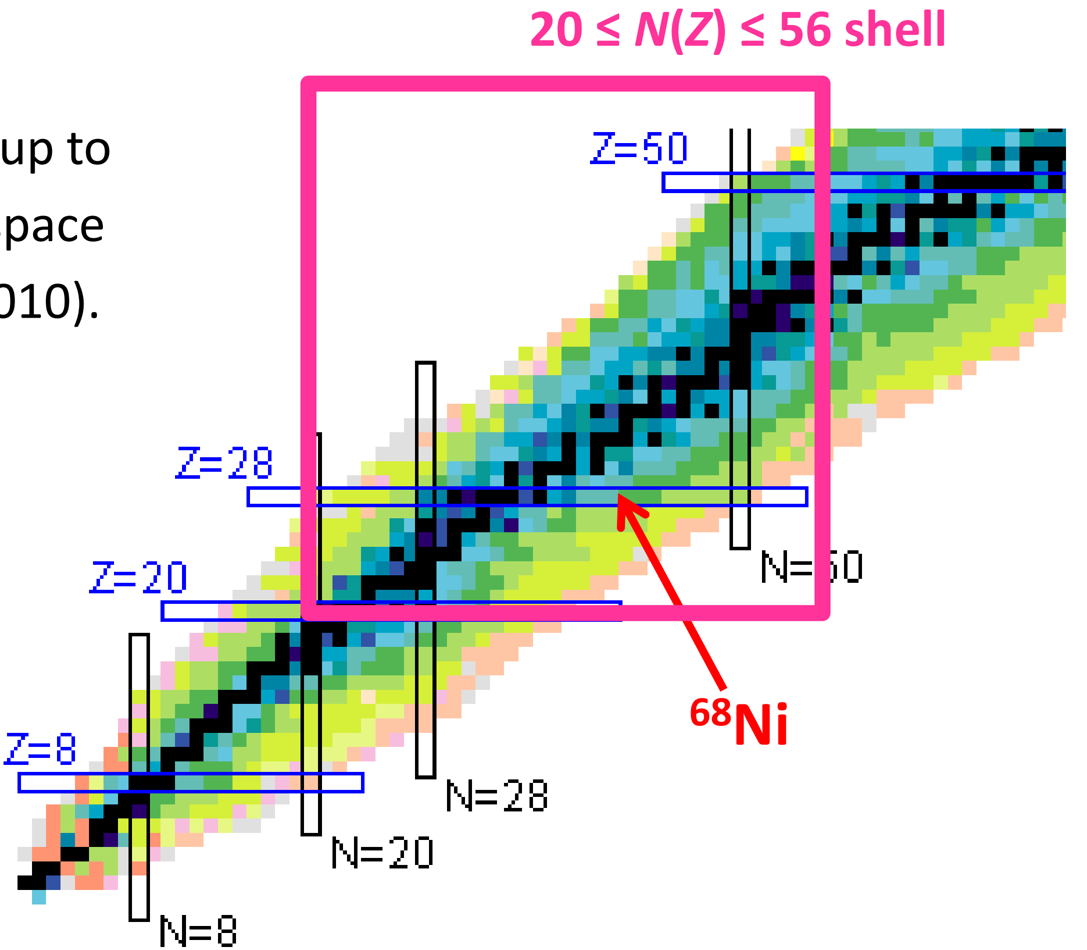

Systematic MCSM calculations for Ni isotopes

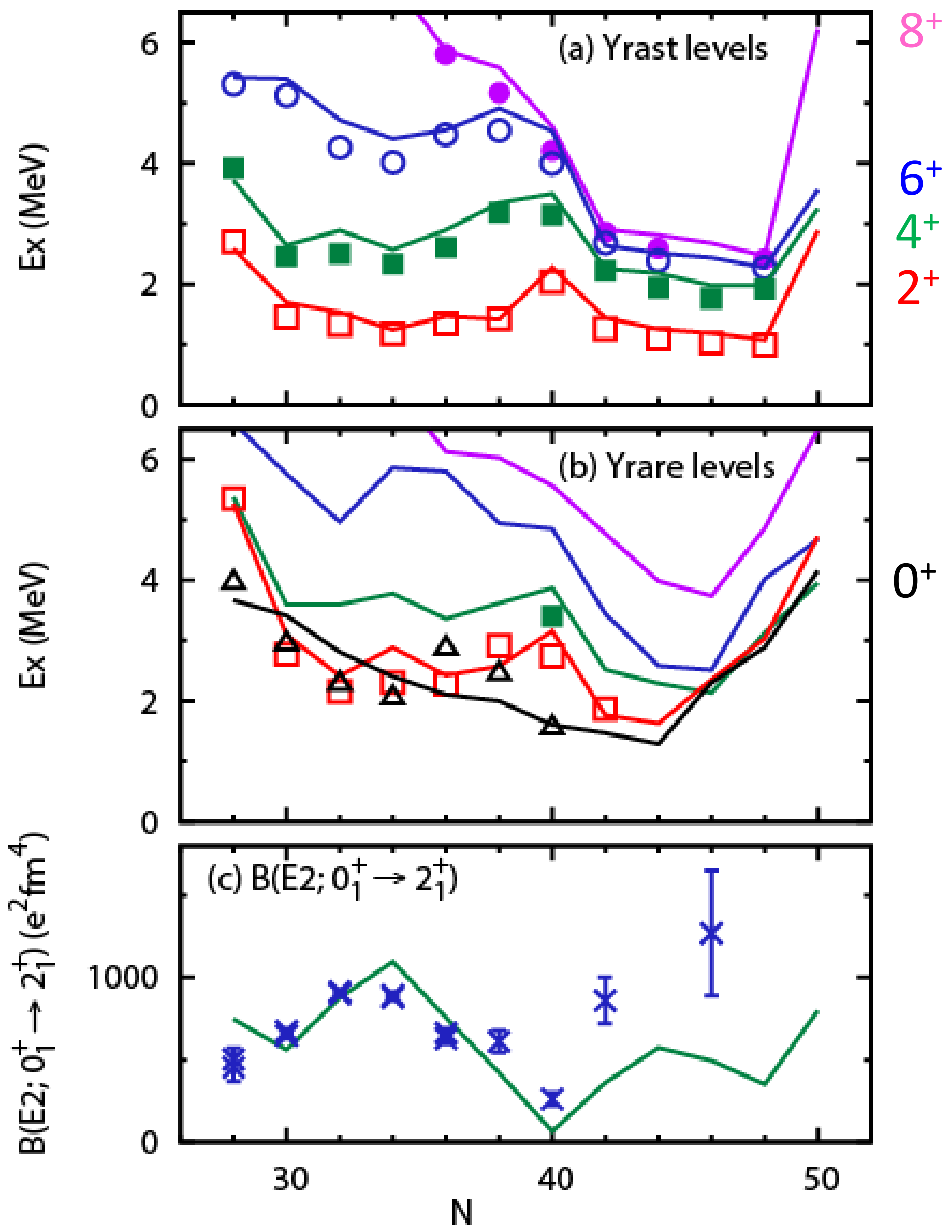

2×10^{10} core·sec ≈ 600 year·core in total

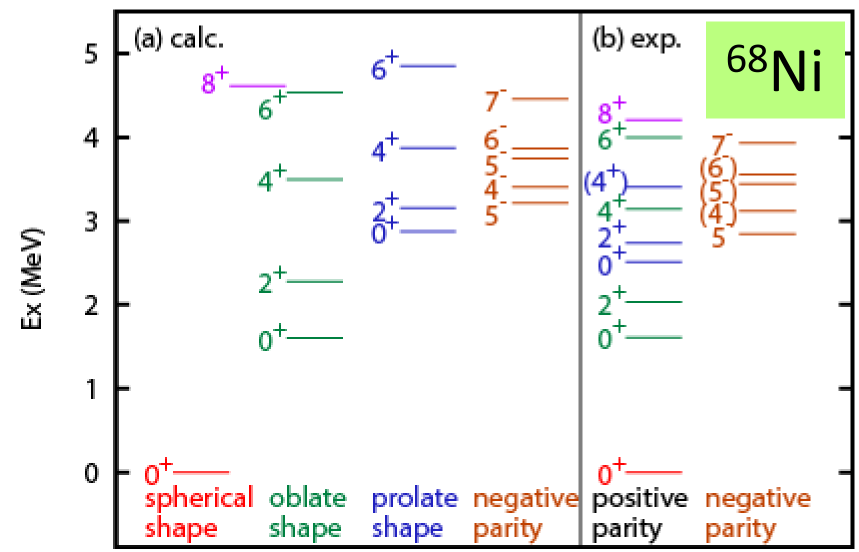

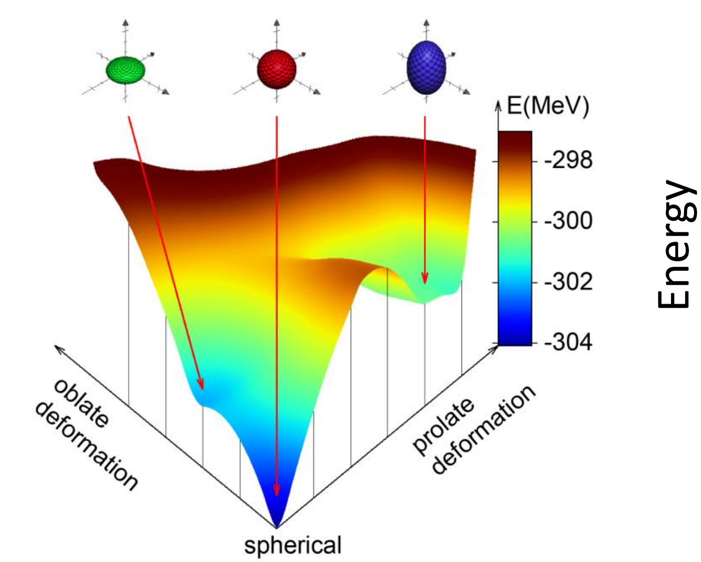

Y. Tsunoda et al., Phys. Rev. C 89, 031301(R) (2014).

Visualizing the shape of MCSM wave function

- Distribution of deformation for the MCSM basis states

$$|\Psi^{IM\pi}(N_b)\rangle = \sum_{d=1}^{N_b} f^{(d)} \sum_{K=-I}^{I} g_K^{(d)} \ \hat{P}^{\pi} \hat{P}^{I}_{MK} |\Phi(D^{(d)})\rangle$$

  – For each basis $|\Phi(D^{(d)})\rangle$ (d=1, 2, ..., N_b),

    - intrinsic quadrupole moments Q_0 and Q_2 ⇨ deformation
    - overlap probability between projected $|\Phi(D^{(d)})\rangle$ and $|\Psi^{IM\pi}(N_b)\rangle$ ⇨ importance

  are calculated.

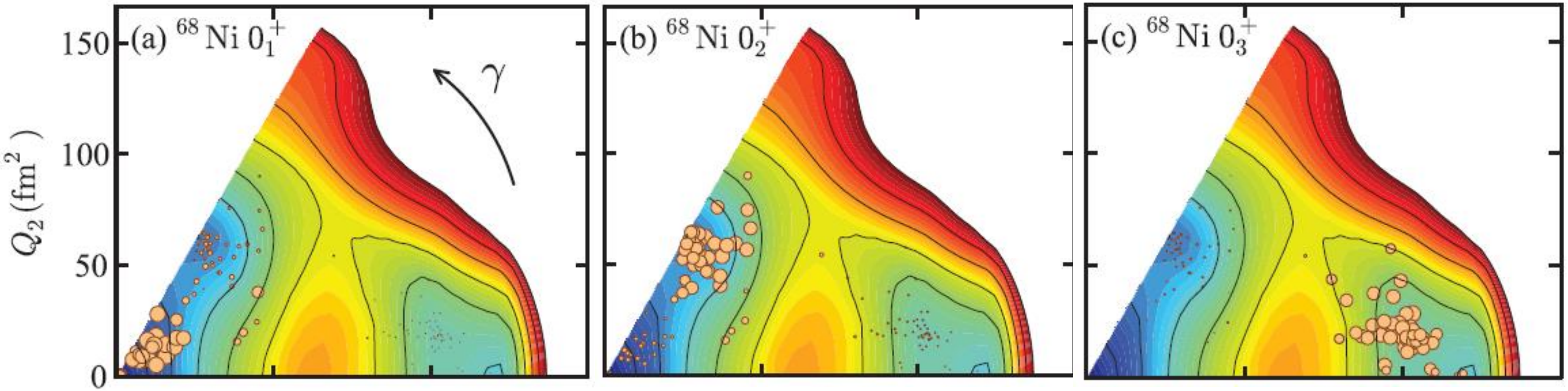

Tensor force: stabilizing deformation

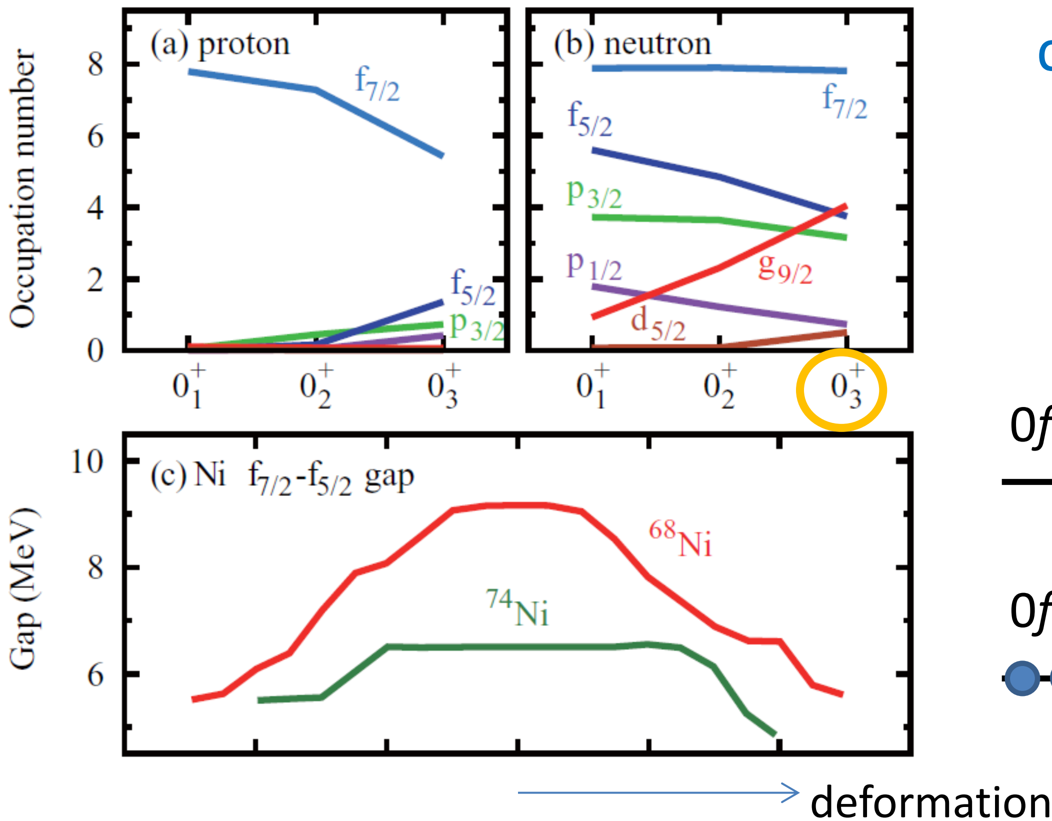

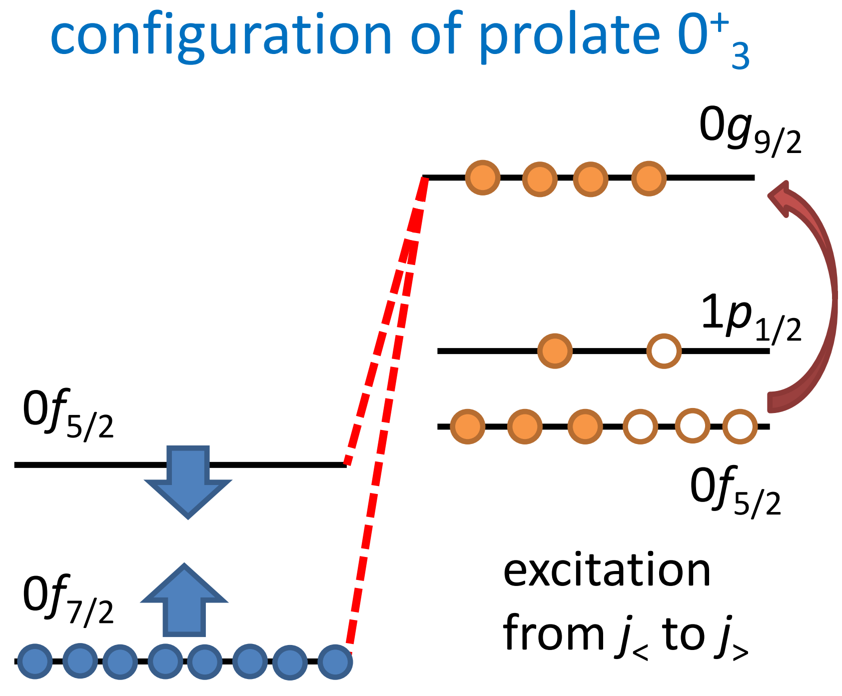

Contrary to the conventional potential picture, the spherical mean field can be different inside a nucleus. In ^{68}Ni, neutron-excited configurations give a reduced spin-orbit splitting, enhancing the Jahn-Teller effect and thus more stabilizing deformation.

Summary

- Shell evolution is investigated with large-scale shell-model calculations.
- Neutron-rich *N*=28 region
  - Direct evidence for the change of spin-orbit splitting due to the tensor force
  - Disappearance of the *N*=28 magic number in ^{42}Si
    - Tensor-force driven Jahn-Teller effect
  - Appearance of the *N*=34 magic number at Ca and its possible persistence toward smaller *Z*
- Monte Carlo shell-model calculations for exotic Ni isotopes
  - Triple shape coexistence in ^{68}Ni
    - Need for a large model space
    - Analysis of shape from the MCSM wave function
    - Configuration-dependent (which we call Type II) shell evolution